SIMPLIFIED MODEL FOR RUBBER FRICTION TO STUDY THE EFFECT OF

DIRECT AND INDIRECT DMA TEST RESULTS

A Thesis

Presented to

The Graduate Faculty of The University of Akron

In Partial Fulfillment

of the Requirements for the Degree

Master of Science in Mechanical Engineering

Michael Kelly

August, 2021

SIMPLIFIED MODEL FOR RUBBER FRICTION TO STUDY THE EFFECT OF

DIRECT AND INDIRECT DMA TEST RESULTS

Michael Kelly

Thesis

Approved: Accepted:

_____   _____
Advisor   Department Chair
Dr. Siamak Farhad   Dr. Sergio D. Felicelli

_____   _____
Committee Member   Interim Dean of the College
Dr. Alex Povitsky   Dr. Craig Menzemer

_____   _____
Committee Member   Interim Director, Graduate School
Dr. Shing-Chung Josh Wong   Dr. Marnie Saunders

                                         _____
                                         Date

ABSTRACT

The viscoelastic properties of rubber have allowed compounds to be utilized across many different industries. Rubber is a very unique material, and the chosen manufacturing process can result in numerous variations of the polymer. With many potential outcomes, it is crucial to accurately determine the physical attributes of the polymer. For many applications, but specifically for the tire industry, one of the standard methods for determining viscoelastic properties is through dynamic mechanical analysis (DMA). The raw data from DMA is adjusted through the Williams, Landel, and Ferry (WLF) shift equation to create a master curve for the rubber specimen. This study investigates methods for the calculation of friction coefficient, and suggests a new code to predict the friction coefficient. Several discussions in the paper will be for validation of the code and its range of applications. We then implement a parametric analysis to determine which factors critically affect the friction factor results. By finding the sensitivity of the inputs to the new code for friction coefficient, the critical inputs can be identified. The parameters that are studied are the storage modulus, loss modulus, surface asperities heights, the surface asperities wavelength, and the adhesive contribution to friction. The adhesion and hysteresis contributions to the friction coefficient are also discussed in this paper. It is shown that the adhesive contribution plays a large role in determining the friction coefficient. The data from the study will determine the effect that direct DMA testing has

on the friction coefficient as well as tire performance indicators. The indicators that the direct testing affects the most are the wet traction indicator, the snow traction indicator, and the ice traction indicator.

DEDICATION

To my wife, Yirka, who gave me endless support while we worked through covid, I took on a new job, we planned our wedding, and she sacrificed quality time in order for me to work through my degree. I cannot thank her enough.

ACKNOWLEDGEMENT

I would like to express my appreciation to my advisor Dr. Siamak Farhad for his guidance and support through the course of my thesis. The past year and a half has been an unprecedented time in the world. The global pandemic affected everyone and caused a shut down for many of us across the globe. Again, I would like to thank my advisor for continuing communications through this time with assistance and encouragement.

I would also like to thank my committee members alphabetically, Dr. Alex Povitsky and Dr. Shing-Chung Josh Wong. Thank you for taking the time out of your days in order to listen to work I have completed for this study. I'm excited to share this work with you and finish this endeavor. I look forward to hearing any feedback or suggestions that you may have.

TABLE OF CONTENTS

LIST OF FIGURES

LIST OF TABLES

CHAPTER I

INTRODUCTION

1.1 Tires

Throughout history wheels have been utilized to facilitate transport and support civilization. Wheels date back to BC, and have been used throughout numerous industries, Wheels on chariots, potter's wheels, and water wheel are just a few of the many applications. Today when a wheel is brought up most likely the conversation is actually about a tire. The tire is one of the most mechanically important parts on an automobile. Tires transfer the power generated from the engine to the road and provide stability while maneuvering.

The primary function of the tire is to allow the driver to maintain control of the vehicle at all times. This may seem like a simple task, but when one considers the many different driving maneuvers and varying road conditions that are experienced, the task becomes complex quickly. Not only do tires need to provide enough traction on snow and a wet road, but they also need to minimize rolling resistance to provide greater fuel economy. Tires are highly engineered products, and researchers and manufacturers strategically design tires to develop performance to beat the competition.

1.2 Safety implications

The predominant function of a tire is to ensure the safety of the end user, by allowing them to maneuver the vehicle as needed. If a tire cannot provide the appropriate amount of friction to the road surface driving conditions can become dangerous. There are numerous examples of conditions that reduce friction, but the most commonly analyzed road conditions are snow traction and wet traction. Other issues that can reduce the friction provided by tire tread, are tires with low pressure, low tire tread, and worn tire tread through a combination of mechanical where and exposure to the atmosphere. When the road conditions are poor, or tires are worn out any number out unintended instances can occur. Two quick examples of accidents which occur during a turning scenario that can result from poor friction of tires are slide outs and tail spins. In the former the front tires on the vehicle have a lower friction output relative to the rear. Here the car will not be able to complete the turn and simply slide out of the turn. In the later, the rear tires have the lower relative friction. This is the more dangerous case, because in this instance when instability takes over during the turn, the vehicle will lose control and spin out. With these examples the importance of good tire performance becomes clear. In order to design and engineer a tire that maximizes driver safety, an understanding of the mechanical properties of the tire's materials is crucial.

1.3 Materials used in tires

Consumer tires are typically radial and tubeless. A tubeless tire maintains air pressure through an impermeable innerliner. This innerliner is typically made of a viscous rubber such as a butyl blend. The radial characteristic of a tire refers to the use of a radial ply. A radial ply is a set of parallel cords oriented perpendicular to the circumference of the tire. This is just one of the many layers and other mechanical structures included in a tire.

Tires are a highly engineered product comprised of more than just rubber. A tire is comprised of six components: bead, belts, body ply, sidewall, innerliner, and tread. The bead is a collection of metal wires that anchor the plies of the tire and helps the tire maintain contact with the wheel. The belts and plies of the tire are held in tension and help maintain inflation pressure. The innerliner, generally comprised of two sheet-like layers of a viscous rubber, stops air from permeating out of the tire and helps maintain the pressure. The sidewall protects the body ply and other components from physical damage and attack from ozone and oxygen. The purpose of the tread is to maintain friction with low rolling resistance and resist wear and tear. Tread wear resistance has three benefits: maintaining ideal friction conditions, protecting the belts, and increasing tire longevity [41]. Tire manufacturers utilize different materials and designs to achieve the desired performance in each component of the tire, but one of the primary raw materials used throughout the industry is rubber.

1.4 Rubber

Rubber is used in many applications, such as medical devices, wires and cables, damping systems, and consumer products such as shoes [7]. This polymer is used in almost every aspect of the tire, from the inner liner, side wall, belts, and plies to the tire tread. Tire companies can work with synthetic rubber or natural rubber and will choose different types of rubber depending on the application and performance requirements of each component [16]. For tire treads, rubber is chosen for its viscoelastic properties. The elasticity of rubber helps the tire tread to absorb the energy of the deformations from rolling and propel the tire forward. The viscous properties of rubber also contribute to the friction of the tire. The correct choice of rubber is paramount for developing a tire that allows the driver to maintain control of the vehicle in adverse road conditions. A number of choices in the manufacturing process must be considered in order to develop rubber with the desired mechanical properties.

1.5 The manufacturing process of tire tread

1.5.1 Base

Some of the polymers used to craft tires today are butadiene rubber, natural rubber, and styrene butadiene rubber. As the name suggests, natural rubber is a material that occurs in nature [16]. Originally, natural rubber was the only option available, modern manufacturers have many options for creating a polymer optimized for an applicatoin. Choosing a base for a tire tread is the first step in determining the proper recipe. The base material is commonly comprised of a blend of multiple polymers.

4

Another common practice is to use styrene butadiene as the base of the tire tread [7]. These polymers can be optimized through the use of fillers and additives and vulcanization.

1.5.2   Fillers

Carbon black and silica are common fillers used within tire tread [7, 16]. Fillers function to provide the polymer with improved mechanical properties for given applications. For example, increasing the amount of carbon black in the polymer will increase the hardness, elastic modulus, and the spring rate for the material. The same is also true for the abrasion resistance of the material, but the benefits will hit an optimum value before entering the realm of diminishing returns [6].

Before Michelin introduced "green tire technology" to the tire industry, there was a limit to what fillers could accomplish in a tire. There was a limit to how much rolling resistance or wet traction could be improved without diminishing other performance aspects of the tire. However, when Michelin began to use silica as a filler, they were able to not only reduce rolling resistance, but also increase the wet traction for tire tread [16] The only problem with using silica was its polarity, which made it less compatible with the base material. For more detail on this phenomenon see [16].This often manifests as poor dispersion in the base material, although manufactures can mitigate this by adding silane coupling agents during the mixing process [16]. In some cases, a mix of both carbon black and silica is used in the same compound.

Today, companies are focused on creating a greener tire as well as finding ways to optimize interactions between the base material and the chosen additives. Epoxidized

natural rubber tire treads were created in an attempt to reduce the carbon footprint of the

tire. These tires were also silica filled. Compared to other tires, the epoxidized natural

rubber tire treads had much better rolling resistance and wet traction performance [23].

The tire will continue to evolve, and companies will continue to implement new solutions

to improve performance and cut down on the ecological impact of the tire.

1.5.3 Oils

Oils or plasticizers, such as petroleum oils, are commonly used in the

manufacturing of rubber compounds [12]. The addition of oil can have multiple effects

on the material. In general, oils tend to shift the glass transition temperature (Tg) of the

polymer, the viscoelastic properties of the material, and even assist in the processing of

the polymer [6]. Oils can allow the material to flow more smoothly and allow fillers to

disperse more evenly, overall increasing the processability of the material. Regarding

shifting the Tg of the material, oils tend to reduce Tg as well as broadening its range. The

lower the solubility of the oil, the more efficient it will be at broadening the Tg range.

This broadening of the Tg improves the polymers performance for tread applications. In

addition to improving these parameters oil may also affect the modulus and hardness of

the material [6].

As previously mentioned, one of the most predominant trends in the

industry is the quest to create a more eco-friendly tire. The industry is seeking to

accomplish this at every level of the manufacturing process. In regard to plasticizers, tire

manufacturers are using bio-oils to alter the performance of tread compounds [12]. A

study analyzing the feasibilities of bio-oils found that the bio-oils were similar to the

control oils. In some instances, the new oils, such as orange oil, led to improvements in dry handling, but had less favorable results in snow traction. The industry will continue to analyze bio-oils and investigate which options offer the most favorable reactions and which can be leveraged to improve tire treads.

1.5.4   Mix Times

Mixing times and schedules is another factor which can be manipulated to vary the material properties of the rubber product. It has been shown that for natural rubber filled with silica, changing the mixer temperature settings and the time between mixing intervals can greatly alter the dump temperature as well increasing the compatibility between the base and the filler [16]. The viscoelastic properties of the material have shown to be affected by the dump temperature. One of the ways to increase the dump temperature is to increase the internal mixer temperature. As the dump temperature increases the $\tan(\delta)$ for silica filled natural rubber will actually decrease to a final low point and then hold. For different combinations of mixtures and fillers these effects will vary over the range of dump temperatures. It is important to optimize the mixing schedule and recipe for the chosen materials and intended use.

1.6 Determination of material properties

1.6.1   Viscoelastic material

In general, the two basic material distinctions are elastic materials and viscous materials. Considering an ideally elastic material, we can quote Robert Hooke from 1678,

"The power of any spring in in the same proportion with the tension thereof." In other words, there is a linear relationship between the stress applied to a material and the strain observed, or vice versa. The elastic modulus of the material, or the stiffness, is calculated as the ratio of the stress response over the strain. The elastic modulus is also known as the proportionality constant from Hooke's Law which is seen below [6].

$$\sigma = E \times \varepsilon \tag{1}$$

Hooke's Law above applies to a perfectly elastic material. In the above equation, σ is stress, and ε is the strain. E is the elastic modulus for the material. Metal springs are one such material that provides a representation of a perfectly elastic material [6].

In addition to elastic material properties, most materials have a viscous behavior. Here when we consider a perfectly viscous response, this attributed to Newtonian fluids such as water. These Newtonian fluids, or ideal fluids, follow Newton's law seen below [8].

$$\sigma = \eta * \dot{\varepsilon} \tag{2}$$

In this equation, σ is stress, η is the viscosity of the material, and ε˙ is the strain rate with respect to time. The viscous response of the material is a measure of the flow of the material. Whereas the elastic response is attributed to energy storage, the viscous response correlates to energy dissipation. Here, energy is expended, deforming the material, and is dissipated or lost through heat generation.

The basic imagery related to the theory is the bouncing ball. When a rubber ball is dropped, it will hit the floor and rebound, but it will not reach its original height. Here you can see the direct translation of the spring and dashpot model. The spring, which represents the elastic response in this model, is related to the amount of energy stored by the material and then released, just as the stored energy will determine how high the ball bounces. The dashpot portion of this model demonstrates to the amount of energy that a material will lose by converting it to heat. The reason the ball never reaches the initial position is due to the energy loss [8]. The viscous response of a material is one of the contributors of friction generation.

Many materials exhibit both viscous and elastic material responses and are not perfect representations of either. When both types of response are observed in a material, it is often classified as a viscoelastic material. Polymers, such as the rubber materials used in manufacturing tires, are viscoelastic materials. These materials contain both crystalline and amorphous regions. These materials are generally composed of numerous tangled long chains of molecules [8].

Maxwell   Voigt
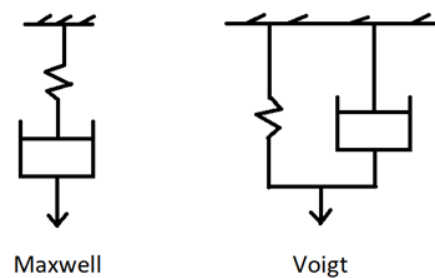
Figure **1-1**: Viscoelastic material models.

For mathematical modelling, viscoelastic materials are typically represented as a combination of a spring and dashpot. The two basic representations, called the Maxwell model and Voight model, are shown in figure 1-1 [6]. For basic applications, such as creep response or the stress relaxation of a material, the Voight and Maxwell models are used, respectively. In the mathematic modelling of a material, typically one of these models is set in parallel with additional springs or combinations of springs and dashpots. These combinations will depend on the material in question, and which combinations accurately represent the material response [8]. An understanding of the viscoelastic response of a material is paramount to select the best material for a chosen application. The viscoelastic properties of the material not only indicate the final material properties, but also help predict how the material will behave during processing and mixing [6]. Each rubber component of a tire, such as the tread, innerliner, or sidewall, requires specific material properties to accomplish its function.

1.6.2   Dynamic mechanical analysis

Dynamic mechanical analysis (DMA) is one of the standard methods utilized to determine the viscoelastic properties of a given material. DMA can be used to analyze polymers, polymer composites, rubbers, epoxies, and even some polyurethane [7]. This type of testing generally consisted of sinusoidal deformations of the material, accompanied with a temperature sweep. The casual observer can look at a generic tension or compression test and witness a lag between the signals of stress and strain. For example, in a standard cyclic tension test, you will see two different sine curves while analyzing the data, one for the load or stress and the other for deformation or strain,

provided that the chosen test is using a sine wave as the deformation control. Using the results from a DMA test, one can determine the viscoelastic properties of the material. The data during a DMA test is the complex modulus (E*) and the phase angle (δ) between the sin waves for stress and strain. The storage modulus (E') and loss modulus (E") are then calculated from these components. The best way to conceptualize this is shown in the right triangle seen in Figure 1-2.
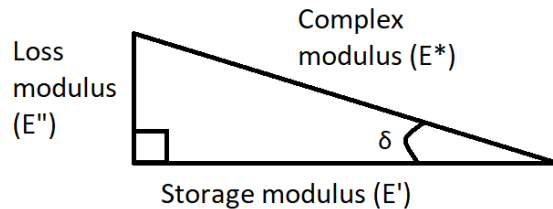
Figure **1-2**: Geometric relationship of viscoelastic properties.

The relationships between the loss modulus, storage modulus, δ, and the complex modulus are identical as the geometric relationships shown in the triangle above. For a viscoelastic material, the measured complex modulus is composed of both the loss modulus and the storage modulus. These moduli correspond to the viscous and elastic responses of the material, respectively. In turn, with the results from the DMA testing, researchers can predict the storage and damping properties for the material at a given frequency and temperature.

The tan(δ) is an important metric when considering the performance of tire tread. Tan(δ) is the ratio of the loss modulus over the storage modulus, and it is the measure of the material's damping capabilities. A high tan(δ) is representative of high energy

dissipation and is ideal for applications where elevated traction is desired. A low value of tan(δ) translates to high levels of rebound in the material and is needed to reduce certain factors like rolling resistance [6].

One of the other important material properties derived from DMA data is the glass transition temperature (Tg). This is the temperature at which the chains in the polymer begin to move and the polymer starts to behave with a viscoelastic response. At temperatures below the Tg, the material expresses almost purely elastic or glassy behavior. There are three standard methods for determining the Tg of a material from a DMA curve. The first is the maximum value of the tan(δ) curve, the second is to use the extrapolated onset of the storage modulus, and the third is to use the maximum of the loss modulus curve. Below are some estimated Tgs for common rubbers as well as an example of a generic DMA test curve. The curve shows the extrapolated onset of the storage modulus as well as the tan(δ) peak.
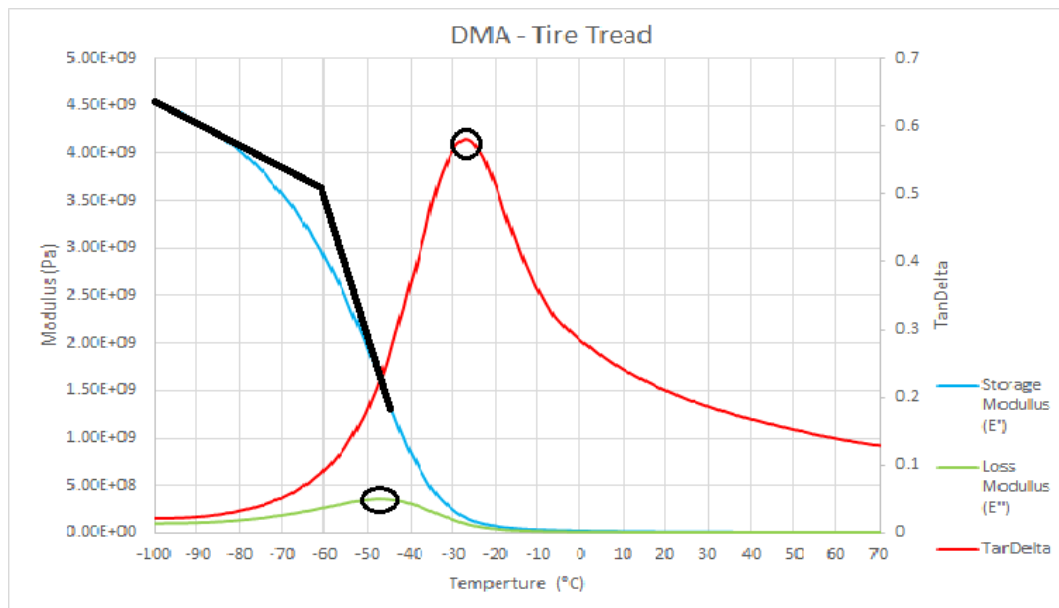
Figure **1-3**: Example of DMA testing I conducted and created of a tire tread in tension mode. Three Tg indicators are shown in the image above, extrapolated onset of the storage modulus, and the peaks of the loss modulus and tan(δ).

1.6.3   Williams, Landel, and Ferry

The Williams, Landel, and Ferry (WLF) relation describes the dependence of the segmental motion of a polymer on temperature [7]. Higher temperatures lead to more thermal energy being available to the material, allowing internal chains to move and respond more rapidly, with the opposite being true for lower temperatures. This response time and the shifts seen with the change in temperature is a phenomenon called the time-temperature superposition principle [20]. The WLF equation can be used to predict this behavior in a given material. A practical application is to use the WLF equation to model the mechanical response of a material under conditions that cannot be physically tested.

For many industries, and especially for the automotive industry, being able to predict the response of a material over a range of frequencies is paramount. The tire is crucial to allowing a driver to maintain control of the vehicle. A vehicle can experience a variety of hazardous conditions while in service, such as rainy or snowy driving conditions or a situation where extreme maneuvering is needed. When conditions such as these occur, the tire tread needs to perform properly to maintain a non-slip condition with the road surface. The tire will experience anywhere from hundreds to hundreds of thousands of cyclic deformations in icy conditions. Realistically, each and every one of these hypothetical conditions cannot be directly tested and modeled, so the tire industry relies on the WLF equation to generate data and model mechanical properties within those frequency ranges.

$$\log(a_t) = \frac{-C_1(T-T_r)}{C_2+T-T_r} \tag{3}$$

In this equation, a_t refers to the horizontal shift factor, and C_1 and C_2 are constants used to finetune the alignment of the generated master curve. Generally, these constants can be set to 17.4 and 51.6 respectively, although they can be adjusted to suit a specific polymer [39]. T refers to the test temperature, and T_r refers to the reference temperature, which can be set to 23°C. This equation is generally used to create a master curve for a polymer's viscoelastic properties. In a master curve, the material's viscoelastic properties are plotted versus multiple decades of frequency. This allows one to gage the mechanical response of the material at the frequencies the polymer will experience during extreme driving conditions. In general, testing begins at low temperature and frequency. These variables are then increased over time to simulate ambient temperatures and high frequencies. Multiple DMA tests are conducted at different temperatures, and that data is used to generate the horizontal shift factor for each of the temperatures tested. The two constants of equation (3) can be optimized to create a smooth master curve.
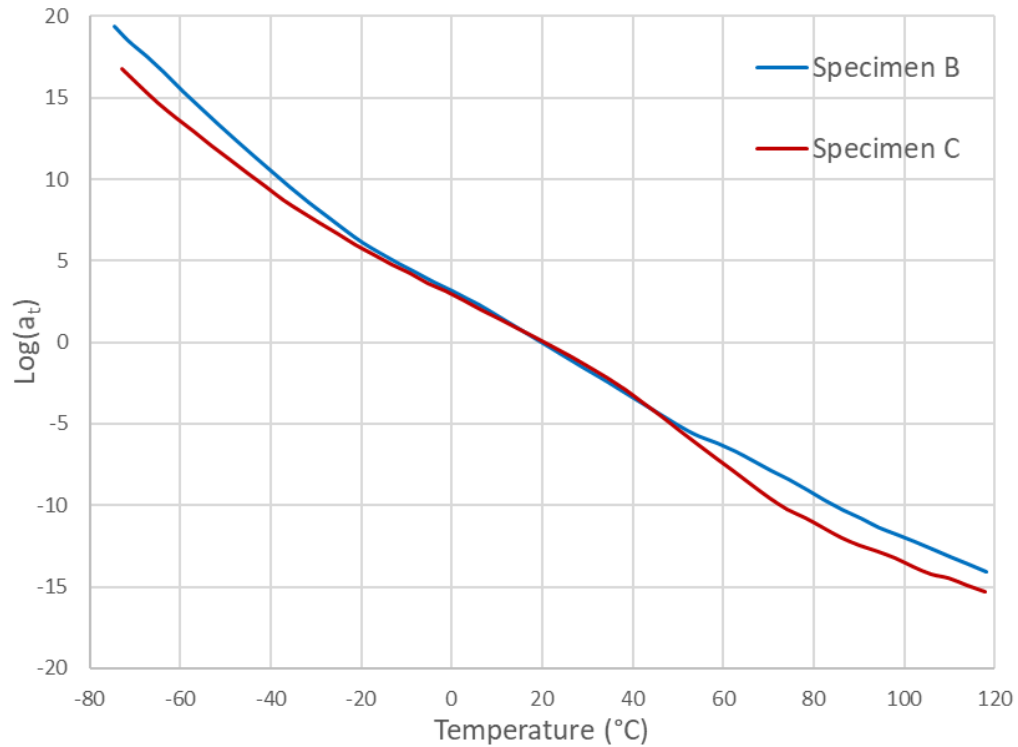
Figure **1-4**: This graph depicts the horizontal shift factor calculated using the WLF equation. This figure shows the WLF equation results for the 2 different tread materials used in the study.
Note: This figure was adapted from Tolpekina, T. V., and B N. J. Persson. "Adhesion and Friction for Three Tire Tread Compounds." *An Open Access Journal from MDPI*, Apollo Tyres Global R&D, 26 Feb. 2019, www.mdpi.com/journal/lubricants.

1.6.4   High frequency DMA

The viscoelastic properties of a polymer are important for determining its

performance. Testing data is processed and shifted using the WLF equation to determine

the mechanical reaction at high frequencies [7]. The WLF shift method has a few

limitations and is limited to the temperature range of Tg + 100°C. To improve upon the

current DMA testing techniques, Roja Esmaeeli worked to develop a new machine to

conduct DMA testing [7]. This machine utilizes a piezoelectric actuator and tests

materials in shear configuration. The new machine has a frequency range up to 5000, and

its travel is 15 µm. This is a frequency five times higher than the quickest commercial

testers [7]. Esmaeeli's team refers to the new machine as a high frequency DMA tester

(HFDMA).

In order to verify the HFDMA, the team conducted a gauge repeatability and

reproducibility analysis. The group used Minitab@ statistical software to perform the

computational side of the analysis. The system was found to have statistical

reproducibility and was capable of accurately conducting DMA testing at high

frequencies. With this new device, researchers can get closer to direct testing and rely

less on the time temperature superposition (TTS) and the WLF relation.

II CHAPTER

LITERATURE REVIEW

2.1 Literature review

Friction has been studied throughout the years, and the theories are ever changing overtime. With the need to continually improve and enhance products, companies and research groups alike have been working to push this field forward. In this study, we consider the friction coefficient for rubber materials used in application such as tire tread. In general, the frictional force experienced by rubber can be summed up by two main factors, the friction caused by the hysteresis of the rubber and the adhesion of the rubber in contact with the surface of the substrate [37].

In the recent study [37], the team analyzed a rubber block sliding on safety tape to simulate a rough surface. To conduct the experiment, a friction tester attached to a load cell to accurately record the frictional force recorded throughout the test. The specimen was a rubber block with a static load applied evenly over the top surface of the rubber. In the experiment they tested for both wet and dry surfaces. The friction coefficient was lower in the wet condition, and this was attributed to the loss of the adhesive contribution for friction [37].

Here Tanaka et al used a Persson methodology to compute the friction coefficient [37]. In this method the team incorporated the power spectrum for the surface roughness, selections for the optimized wavelength and magnification, the viscoelastic properties of the material, and the actual area of contact between the rubber and the surface. The team also incorporated a scaling parameter β, to account for the nonlinear behaviors of the viscoelastic properties of rubber. The aforementioned equation for the hysteretic friction coefficient was combined with the adhesive friction coefficient, a function of the real contact area and the ratio of the shear stress to the applied stress on the material. In these results, the calculated friction coefficients agreed well at lower sliding velocities, however as the sliding velocity increases the model begins to overestimate the measured friction coefficient [37].

In a study conducted by Tolpekina and Persson [39], analyzed three different materials and tested their model against experimental data. The equations they developed can be seen in chapter III of this psper, and are very similar to those developed by Tanaka et al. The most noticeable difference here is an addition of a coefficient of friction constant, set at 0.2 for this study. The researchers attributed the need for this additional constant to the extra fiction caused by the filler particles scratching the ground. The results from the study show a good trend between the experimental and calculated results for dry friction. Like we have seen in the previously discussed study by Tanaka, the purely hysteretic component of friction falls below the experimental value for the experimental data for wet friction [39]. This indicates that the adhesive friction contribution should not be fully ignored when considering wet traction.
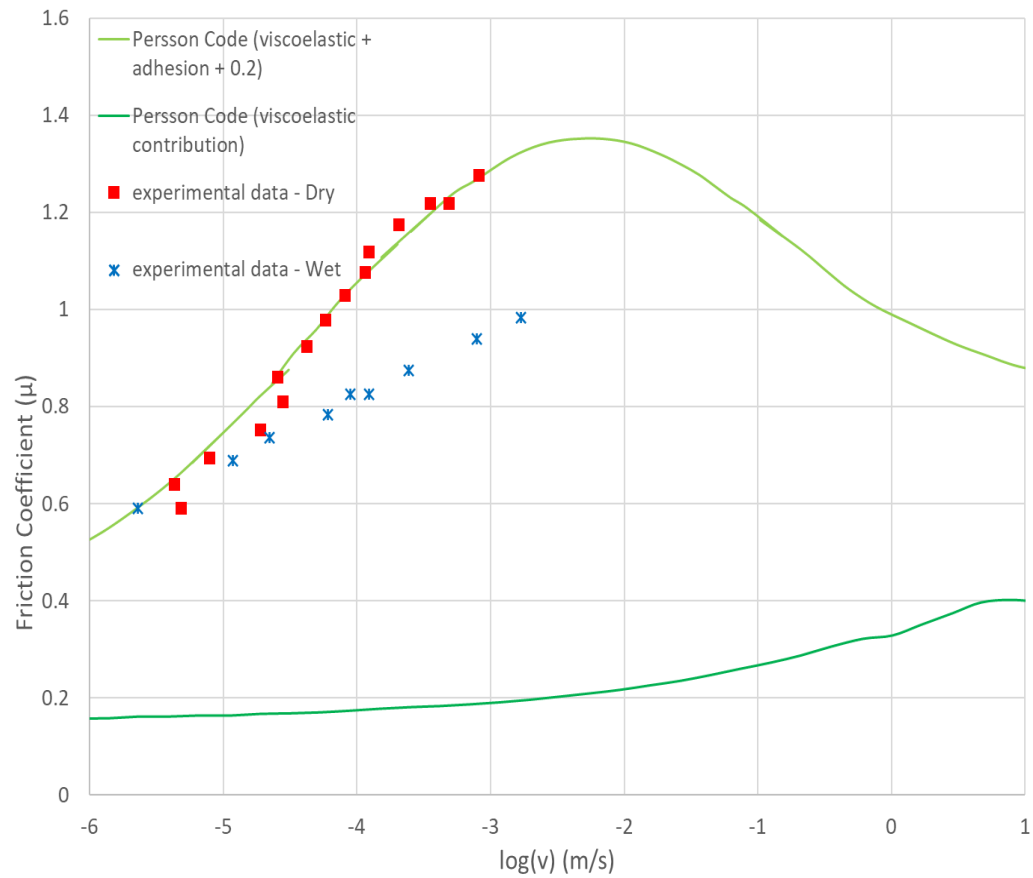
Figure **2-1**: The results for the total and hysteretic friction coefficients (upper and lower green lines) are displayed against the experimental data.
Note: This figure was adapted from Tolpekina, T. V., and B N. J. Persson. "Adhesion and Friction for Three Tire Tread Compounds." *An Open Access Journal from MDPI*, Apollo Tyres Global R&D, 26 Feb. 2019, www.mdpi.com/journal/lubricants

2.2 Research gaps

Understanding rubber friction is an ongoing process, that is chipped away at by different teams of researchers. We have found that even for a very basic application of a rubber block sliding over a rough surface modeling still is not capturing the data perfectly. When trying to account for the nonlinearity of rubber it was found that optimizing the upper wave cut-off number and adding a scaling factor on the calculation of real contact area, were not capable to fully capture the behavior of the rubber [37].

The calculations seen in the mentioned studies required rigorous computations over multiple integrals. Dealing with, in many cases multiple integrals, and choices on magnification and wavenumber cutoff. Another study that we discuss in the next section of this paper works at a simplified version of the calculation of the hysteretic or viscous friction coefficient. With the simplified code utilizing just the slope of the real mean squared value for the surface height variation (h'_{rms}), the loss modulus, and the complex modulus of the material [5]. In the study the author tested his code against one study and found the simplified code to match Persson's code rather well [5]. However, this Ciavarella code still needs to be verified against the results of additional studies to gage its validity.

Aside from the two areas listed above, another opportunity for improvement is in the area of the WLF and TTS equations. Again, this principal utilizes the concept that material properties found at colder temperatures shift towards the corresponding material response at higher frequencies [43]. Although these principals have been established, they do have some short comings. In some cases, the master curves can't be recreated for

20

certain polymers. For example, in some crystalline polymers there are chains that from out of place in the network. These chains can create internally overlapping friction generators, in turn allowing for multiple transitions within the same temperature zone expanding the transition regions and making it harder to characterize [7, 20]. These crystalline polymers with thermorheological intricacy are one example of where the WLF equation can cause some complications. For polymers such as these, sometimes a vertical shift is also necessary to obtain. The differences in material density or thermal expansion are intended to be accounted for with this vertical shift [20]. This complication has also been seen in some rubber polymers being newly developed. In general, this relationship is also only valid for the temperatures between the T_g and the $T_g + 100°C$ [7]. The new HFDMA is one attempt to alleviate these concerns, and the implantation and construction of the device is detailed in [7]. Some of the next steps moving forward with this technology is to continue to evaluate this type of testing on additional materials and implement the data gathered for additional application

2.3 Confirmation of Ciavarella code

Building off of the work from Persson [29, 30, and 31], scientists have continued and improved upon the understanding of rubber friction. If you consider where most of us started with friction, normal force, and friction coefficients the analysis has evolved and is ever changing. The recent model considered was based off of the many different works of Persson, researching friction and all of the factors that may affect the coefficient of friction for a given material such as rubber. This model considers the roughness of the surface profile, the real contact area of the interaction, and the viscoelastic properties of

21

the chosen material. Based on the roughness of the surface profile and the level of

magnification, you can determine what frequency the material will be subjected to for the

given test speed. With this information, the corresponding material properties can be used

and incorporated into the calculation for the friction coefficient. Persson [21] provides a

very complex equation and involved calculation to determine the hysteretic friction

coefficient. This method considers the surface roughness, the chosen low limit and high

limit for the surface wavenumber cut-offs, and the corresponding magnification values.

With this considered the amount of real contact of the material to the surface is calculated

and incorporated into the calculation of the friction coefficient. In general, the

viscoelastic material properties will come from the master curve for the material derived

from testing.

<div align="center">2.4 Objectives</div>

The objective of this paper is to determine the validity of a simplified code for the

friction coefficient of sliding rubber. This new code is a combination of codes from

multiple studies and research groups. In this study this code will be validated against

experimental data and a parametric analysis is conducted to analyze the sensitivity of the

new code to its variables. With the simplified code, more researchers can investigate this

phenomenon without the high barrier to entry. The reduced computation necessary with

the new code will account for this. An understanding of the relevant parameters can also

help lead tire companies to the right areas to investigate for improving the performance of

their product.

III CHAPTER

MODELING

3.1 Friction Coefficient

3.1.1   Surface Contact

The interactions between a rubber material and a surface have a strong influence on the friction coefficient generated from sliding the material across the surface. Both the number of random oscillations in the surface itself and the sharpness of the slope affect the friction coefficient. These properties also vary based on the level of magnification at which the surface is inspected. Differences in these properties can alter the h'rms of the surface and which portion of the master curve is applicable to model the application.

In order to model a material's response to a given surface, the first step is to analyze the surface itself. Some of the techniques used to inspect different substrates are laser inspection, photogrammetry, and microscopy, microscopy being the most common [7, 37]. One of the parameters used to characterize a surface is the peak-peak distance between the oscillations seen on the surface. Here, analysis has been broken into three different categories for surfaces: micro, macro, and mega textures [7].

Under a higher magnification, the distance between the oscillation peaks is much reduced compared to observations at lower magnifications. For images of different

surface magnifications you can refer to [37]. In this study, safety tape was used to

replicate a rough surface by sliding rubber blocks across lengths of tape. The friction was

recorded, and the surface analysis was utilized to create a code to replicate the measured

friction [37]. The analysis of the surface is necessary for the modeling of friction

generated by sliding across the surface.

3.1.2 Methods for determining friction coefficient

3.1.2.1 Hysteretic

The hysteretic contribution to the coefficient of friction is caused by the energy

loss experienced through the tire tread during driving. Deformation of the rubber tread

due to the interaction with the surface is generally modeled using a spring and dashpot

model, as seen in the base version in figure 1-1. The material undergoes continuous

cycles of compression and relaxation, which leads to energy loss through heat dissipation

in the rubber. While analyzing data, this can be observed through the phase shift in DMA

analysis or in the hysteresis loop in the load versus displacement curve of a single

deformation cycle.

This pattern continues when observing the interaction at different levels of

magnification. As rubber moves across a rough surface, the changes in amplitudes and

distances between corrugation peaks shift as the selected magnification changes. In order

to accurately model frictional losses due to this phenomenon, current literature has

considered that an upper wavenumber cutoff needs to be applied when analyzing rubber

to substrate interactions. This limit is intended to account for the micro scale at which

filled rubber can have inhomogeneous deformation, without assuming uniform dispersion

of filler particle. At certain degrees of magnification, surface contamination and adhesion interactions can also affect the hysteretic behavior of a viscoelastic material such as rubber [21, 37, 39].

This wavenumber cutoff determines what level of magnification should be considered for a given application. This variable is chosen to allow for a strong representation of real-world scenarios while avoiding areas of uncertainty for modelling. The best method for selecting a wavenumber cutoff is unclear and should be determined based not only on surface analysis, but also by the properties of the rubber itself [28, 37]. Another study [5] investigates whether the wavenumber cutoff plays a meaningful role in the resulting coefficient of friction at all. The author claims the process for determining the wavenumber cutoff is unclear and potentially not physically relevant [5]. In this study, we investigate these claims by testing a new simplified code on additional tested data and determine what effect this parameter has on the output of the new simplified code.

3.1.2.2 Adhesive

Aside from the friction generated through hysteretic losses, it is commonly accepted that the second main contribution to the friction coefficient is due to adhesive effects of sliding rubber. As seen in equation (15), the adhesive contribution is the ratio of shear stress over nominal stress multiplied by the ratio of the real contact area of the rubber to the substrate beneath. This shear stress is believed to occur due to microscopic bonds breaking. Some studies have chosen to model at this bond break as crack propagation energy [37]. Naturally, the frictional shear stress is related to the velocity and

temperature at which it occurs. This relation has not been confirmed and needs to be determined through experimentation [39].

The work by Tolpekina and Persson [39] has examined the predominant factors of adhesive contribution on different surfaces. As established, surface roughness plays a role in determining the area of real contact for a contact application and the relevant frequency region of the master curve. In the context of sliding contact on dry surfaces, weak bonds form between the atoms of the substrate and the molecules of the compound. Thermal fluctuations are one of the factors that help to break these weak bonds in low velocity sliding applications. This relation shows that if the velocity is zero, the friction force is miniscule. This theory also attempts to explain the lack of the friction observed at high sliding speeds. When the velocity is high enough, it will limit the rubber's ability to interact with the substrate, and there will be a maximum friction shear stress witnessed at some moderate velocity [39]. In section 3.2 he mathematical process used to determine both the hysteretic and adhesive contributions to friction is presented.

3.2 Model equations

The equation used by Lorenzo and Persson were where this study chose to start analyzing the friction coefficient [21]. These studies initially begin to try and model sliding rubber. In this section all equations that represent one form of a contribution to friction will be referred to as a code. In a paper by Tanaka et al., "Prediction of the Friction Coefficient of Filled Rubber Sliding on Dry and Wet Surfaces with Self-Affine Large Roughness," the team continued investigating modelling sliding rubber on a rough surface. Here, the surface was assumed to have inplane isotropy and to be a self-affine

fractal. Following the process developed by Persson in 2001, with these considerations in

place, Tanaka and the team determined an equation for power spectrum of surface

roughness.

$$C(q) \cong \frac{H}{2\pi} \left(\frac{h_0}{q_0}\right)^2 \left(\frac{q}{q_0}\right)^{-2(H+1)} \tag{4}$$

Here C(q) is the power spectrum of surface roughness. The components that make

up equation (4) are the Hurst exponent (H), the surface height amplitude (h_0) at the lower

wave number cutoff (q_0), and the wavenumber (q). The real amount of rubber in contact

with the surface is the next consideration for this method [37]. The authors simplified the

equation for relative area of real contact by adhering to the following considerations: The

team simplified the equation for relative area of real contact by adhering to the following

considerations: While q is within the range (qo, q1), the nominal stress was much smaller

than the elastic modulus, and the calculation for G(q) was much larger than 1. The

simplified equation is thus:

$$G(q) = \frac{1}{8} \int_{q_0}^{q} dq q^3 C(q) \int_0^{2\pi} d\emptyset \left|\frac{E(qvcos(\emptyset))}{(1-v^2)\sigma_0}\right|^2 \tag{5}$$

$$P(q) \cong \frac{2}{\pi} \int_0^{\infty} dx \, exp(-x^2 G(q)) = (\pi G(q))^{-\frac{1}{2}} \tag{6}$$

In this expression, q and C(q) have the same meaning as previously determined.

The relative area of real contact, P(q) is calculated through the surface analysis of G(q).

Here E(qvcosϕ) is equivalent to the complex elastic modulus in terms of the angular

frequency. In that segment of the equation, v is the velocity (m/s), σ_0 represents the

normal stress, and v on the bottom of the integral is the Poisson's ratio for the material.

Using the above equations, Tanaka developed an equation for the hysteresis coefficient of

friction after adjusting for the fact that the surface is a self-affine fractal. In the equation below, the new terms are the hysteresis friction coefficient (μ_{visc}), and ζ refers to the spatial magnification of the surface [37].

$$\mu_{visc} \cong \frac{1}{4\pi}(q_0 h_0)^2 H \int_1^{\frac{q_1}{q_0}} d\xi \xi^{-2H+1} \left(1 + \left((G(q)^{\frac{3}{2}})^{-\frac{1}{3}} \int_0^{2\pi} d\emptyset \cos(\emptyset) Im \frac{E(\xi q_0 v \cos(\emptyset))}{(1-v^2)\sigma_0}\right)\right) \quad (7)$$

$$G(\xi) = \frac{1}{16\pi}(q_0 h_0)^2 H \int_1^{\frac{q_1}{q_0}} d\xi \xi^{-2H+1} \int_0^{2\pi} d\emptyset \left|\frac{E(\xi q_0 v \cos(\emptyset))}{(1-v^2)\sigma_0}\right|^2 \quad (8)$$

Tanaka et al. used these equations to calculate the hysteresis friction coefficient for a carbon-black filled rubber. These calculated results were then compared to the results generated from the friction experiments conducted on wet and dry surfaces [37]. From this starting point a new method for friction calculations was developed by simplifying the original Persson system of equations (5). The study starts off by generalizing the Persson equation into the form seen below.

$$\mu_{visc}(q_1) \cong \frac{1}{2} \int_{q_0}^{q_1} dq q^3 C(q) S(q) P(q) \int_0^{2\pi} d\emptyset \cos(\emptyset) Im \frac{E(qv\cos(\emptyset))}{(1-v^2)\sigma_0} \quad (9)$$

In equation (9) μ_{visc} refers to the viscous contribution to friction, S(q) is a correction factor ≈ 0.5 at large magnifications, and P(q) is a single variable form for the relative area of real contact. Simplifying this form of the equation was accomplished with the following considerations. With a small lower limit wavenumber cut-off value, it is a reasonable assumption to assume full contact between the rubber and the surface. Full contact will remain until a certain wave number is reached and some amount of separation occurs. In the study the value was denoted as q_f. Simplifying equation (9) is accomplished by applying these considerations.

$$\mu_{visc}(q_f) \approx \frac{1}{2} \int_{q_0}^{q_1} dq q^3 C(q) \int_0^{2\pi} d\emptyset \cos(\emptyset) Im \frac{E(qv\cos(\emptyset))}{(1-v^2)\sigma_0} \quad (10)$$

Next the fractal dimension was set to 2.2, and with this determination, Ciavarella and Tanaka develop the same calculation of area of real contact as seen in equation (6) as in the study by Tanaka et al. Next P(q) is set to $(1/(\pi G))^{-0.5}$ [5]. After the simplification assuming full contact while q is set to q_f, Ciavarella then splits the equation into parts. Each part is then simplified in turn, effectively removing the integrals from the equation see equations (12, 13, and 14).

$$\mu_{visc} \cong \frac{\sqrt{8}}{4\sqrt{\pi}} \int_{q_0}^{q_1} \frac{dq\, q^3 C(q) \int_0^{2\pi} d\emptyset \cos(\emptyset) Im\frac{E(qv\cos(\emptyset))}{(1-v^2)\sigma_0}}{\sqrt{\int_{q_0}^{q} dq\, q^3 C(q) \int_0^{2\pi} d\emptyset \left|\frac{E(qv\cos(\emptyset))}{(1-v^2)\sigma_0}\right|^2}} \tag{11}$$

Ciavarella began simplifying the formula by substituting R_1 as the integral under the square root. For 2D surfaces the gradients of the orthogonal directions are uncorrelated, and the hysteretic friction coefficient can be simplified to what is seen in equation (12). Applying the principles of a spring and dashpot model the final changes were implemented. This model is seen in equation (14) [5]. $ImE(q_1v)$ is the loss modulus of the material, $E(q_1v)$ is denoted as the complex modulus of the material, and h'$_{rms}$ is the real mean squared slope of the surface profile. For most road surfaces, the h'$_{rms}$ can be set to 1.3 [5].

$$\mu_{visc} \cong \frac{R_1}{\sqrt{\pi}} \sqrt{2m_2} = \frac{R_1}{\sqrt{\pi}} h'_{rms} \tag{12}$$

$$R_1 = \frac{\int_0^{2\pi} d\emptyset \cos(\emptyset) ImE(q_1 v\cos(\emptyset))}{\sqrt{\int_0^{2\pi} d\emptyset |E(q_1 v\cos(\emptyset))|^2}} \tag{13}$$

$$\mu \cong h'_{rms} \frac{ImE(q_1v)}{|E(q_1v)|} \tag{14}$$

Equation (14) allows calculation of the coefficient of friction without the numerous integrals. With this simplification, the hysteretic friction coefficient calculated from Persson's method can be easily estimated with an understanding of the surface of the application and an analysis of the viscoelastic properties of the material [5]. This calculation has been developed for low velocity applications. If higher velocities were investigated thermally induced events can occur affecting the friction coefficient. These events could be when the interfacial temperature of the material increases, or the stick-slip vibration that can occur at higher sliding speeds. When the log(velocity) > -2.5 these slip conditions can occur. The friction coefficient decreases as the instability due to slippage increases [37]. This project didn't investigate such conditions.

Later in this study the calculations from Ciavarella are verified. The simplified code from Ciavarella correlated closely to the Persson model. The average error between Persson's and Ciavarella's code was less than 5%. However, neither method for μ_{visc} could accurately replicate the friction values seen in the experimental results.

In order to find a code to replicate experimental results, a combination of the Ciavarella code and a code developed in a study conducted by Tolpekina and Persson in 2019 [39]was utilized in this study. The complete friction coefficient was set to be the hysteretic and adhesive contribution to friction as well as an offset value [39]. The resulting formulation is seen in equation (15).

$$\mu = \mu_{visc} + \frac{\tau_f}{\sigma_0}P(q) + \mu_{const} \tag{15}$$

Here, μ is denoted as the total friction coefficient. The subscripts "visc" and

"const" refer to the viscoelastic and constant contributions to friction, in that order. The

constant contribution to friction, or μ_{const}, is set at 0.2. This additional factor was

attributed to the filler particles used in the tread. These particles, commonly carbon black

or silica, can be used to improve the lifespan of the tire were assumed to be scratching the

surface during sliding, hence adding an additional contribution to friction [39]. The

middle term in the equation is the adhesive contribution, and it is found by taking the

shear stress (τ_f) over the nominal stress (σ_0) and multiplying by the rubber in contact with

the surface at the magnification level of q/q_o. The equation for P(q) is seen below.

$$P(q) = \frac{1}{\sqrt{\pi}} \int_0^{\sqrt{G}} dx e^{\frac{-x^2}{4}} = \text{erf}(\frac{1}{2\sqrt{G}}) \tag{16}$$

G is found to be:

$$G(q) = \frac{1}{8} \int_{q_0}^q dq q^3 C(q) \int_0^{2\pi} d\emptyset \left| \frac{E(qvcos(\emptyset),T_0)}{(1-v^2)\sigma_0} \right|^2 \tag{17}$$

Erf is used to represent the error function. The complex modulus is E(qvcosϕ).

Just as in equation (9), In the denominator of the second integral, v is the Poisson's ratio

for the material. σ_0 is the stress applied to the to the test block [39]. These are all the same

factors and components as seen in Persson's earlier work covered by both Ciavarella and

Tanaka. The shear stress seen in equation (18) is a function of velocity and temperature.

To calculate this value, the coefficient c = 0.17 and v* is set to 1 cm/s in the study [39].

The friction shear stress coefficient for the equation is set between 4 and 8 MPa by

Persson.

$$\tau_f \cong \tau_{f0} \exp\left(-c\left[log_{10}\left(\frac{v}{v^*}\right)\right]^2\right) \qquad (18)$$

In order to overcome the discrepancies seen between the calculations and experimental data in figure 2-1 a code that calculates more than just the hysteretic coefficient of friction need to be used. Both the wet and dry experimental friction coefficients are found to be higher than the calculations for the viscoelastic or the hysteretic friction contribution. This shows that the adhesive contribution of friction cannot be ignored. The code this study utilizes pieces of the codes generated by Ciavarella and Persson. The calculation for the hysteretic friction coefficient is taken from the simplified equation from Ciavarella, and the adhesive contribution is taken from Persson's 2019 code.

$$\mu = 1.3\frac{ImE(q_1v)}{|E(q_1v)|} + \frac{\tau_f}{\sigma_0}P(q) + 0.2 \qquad (19)$$

The following portion of this study details the validation of this new code. The version of the new code seen in equation (19) is investigated against the experimental data from the 2019 Tolpekina and Persson study. Although the calculation for the adhesive contribution to friction is still in its original form, the new code is still much simpler than Persson's. In the future a better understanding of adhesive friction, will allow us to simplify this equation further. The following section shows that DMA testing data and an understanding of the surface roughness will be all that is necessary in order to produce a decent estimate of the friction coefficient.

3.3 Validation of model

This study is meant to test the validity of this code for predicting the coefficient of friction for a material such as rubber. Understanding a material's friction behavior under different circumstances enables the design of materials for specific applications. Using a simplified code and method for the determination of friction coefficient allows more to access this information. With this system, obtaining the master curve of a material, as well as understanding the properties of the surface of the application, will allow the user to calculate the estimated friction coefficient for the material. This is determined by considering the application and test conditions for the material. In these examples, the information from the surface, such as the wavenumber and the velocity of the experiment, can be used to calculate the frequency at which the rubber will experience oscillations. Once this frequency is obtained, the relevant data can be extracted from the master curve, and the corresponding friction coefficient is produced. This code considers the complex and elastic moduli calculated from DMA testing. With a knowledge of the surface roughness, conditions of the application, and the master curve generated through DMA testing, a good representation for the friction of the material can be generated without conducting an actual experiment. Using this simplified calculation can save considerable time for researchers and manufacturers. With some very standard testing, this code can be used to evaluate a material for multiple applications.

3.3.1 Data from literature

The following portion of the paper will validate this simplified code against three sets of data taken from other published studies. The first is the paper by Ciavarella from which this code was derived. Ciavarella's data was originally taken from a study conducted by [21]. The next two sets of data were taken from a new paper by Persson et al. written in 2020. In each of these studies, the teams used master curves for rubber materials in order to generate a result for the coefficient of friction. Each data set was generated using slightly different methods, but all three utilized raw data, used in cohorts with the surface information in order to calculate the friction values and experimentation results.

The first step in the validation process was to extract the relevant data provided by each paper, namely master curve data and calculated or conducted results. This was accomplished using two programs: GetData Graph Digitizer software and WebPlotDigitizer, a Google app. All data was then traced and exported to Microsoft Excel. The master curve data was used to generate the friction coefficient using the simplified code in Excel. A simple linear extrapolation was used to create data points at specific frequencies in order to conduct direct analysis between all sets of data. In order to properly analyze and represent the data, this process had to be repeated numerous times. The following figures were creating by interposing the newly generated friction coefficients back into the results for each of the corresponding studies. This method allows for direct visual comparison of the new simplified code against experimental results. In addition to the visual analysis, an analysis of the error between data sets was calculated and displayed in table 3-1.

Let us first consider how the recreation of the code for the Lorenzo data provided in the Ciavarella paper. The first task was to verify that the provided code matched and verified the results claimed by the study. This was verified and can be seen in Figure 3-1. The graph shows that the friction coefficients align very well. The only variance to account for was to subtract 0.27 from the final value of the calculated coefficient of friction. These minor differences can be attributed to the processing of the master curve data. The paper by Ciavarella did not disclaim how the master curve data was processed, which could also explain the adjustments. Otherwise, both the Ciavarella data and the replicated code show a strong correlation to the calculated friction coefficient from the Lorenz study. Here, the calculated code from Ciavarella is represented using a dashed line for the purpose of ease of visual inspection.
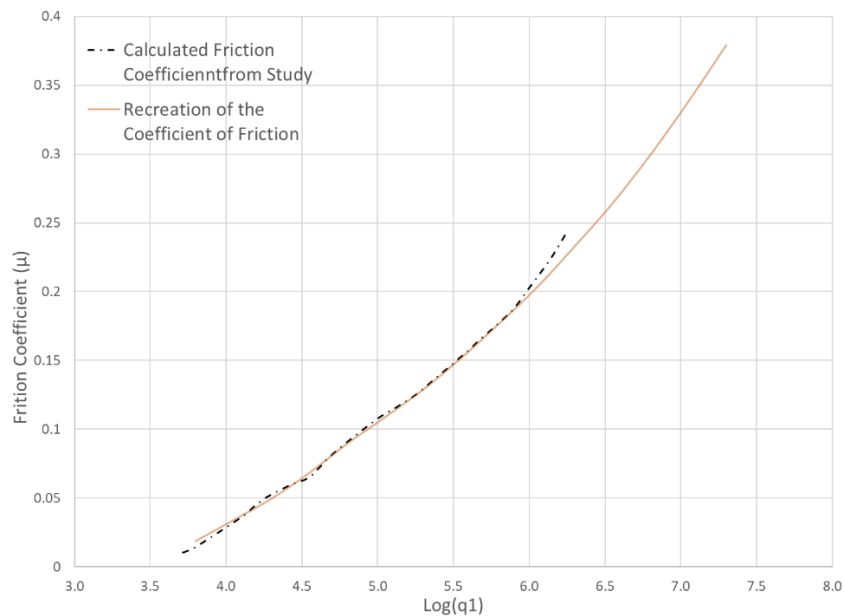
Figure **3-1**: The simplified method for calculating the friction coefficient provided by Ciavarella was calculated and plotted against the original data from the study [5]. Note: This figure was adapted from Ciavarella, M. "A Simplified Version of Persson's Multiscale Theory for Rubber Friction Due to Viscoelastic Losses." Journal of Tribology, vol. 140, no. 1, 2017, doi:10.1115/1.4036917. Originally published by ASME.

From figure 3-1 we can conclude that Ciavarella's simplified code worked as claimed and that our replication of the code was a success. In Ciavarella's paper, he used a study conducted by Lorenz: "Rubber friction on road surfaces: Experiment and theory for low sliding speeds." [22] That study presented the loss and storage moduli for three materials. This data was then used to construct the simplified code for friction coefficient. The next step was to use this code to analyze another set of data. The study conducted by Persson in 2019, "Adhesion and Friction for Three Tire Tread Components," presented the perfect opportunity for validation of the calculation for hysteretic friction. The process for validation against the new study started by gathering the relevant viscoelastic data presented in the study. Persson provided the storage modulus in addition to the calculation for tan(delta) for three separate tire treads. WebPlotDigitizer, a Google app, was used to pull data from the figures found in Persson's study into Microsoft Excel for manipulation. Standard data points were chosen across the frequency range for the data. Once the standard frequencies were chosen and linear interpolation was used to pull out the relevant data at the chosen frequencies, the tan(delta) data and storage modulus were used to calculate the loss modulus for each of the three specimens used in the study. As previously stated, the loss modulus = storage modulus * tan(delta), or E" = E' x tan(delta). This process was completed for specimens B and C from the study. These properties then had to be converted from frequency to sliding velocity in order to compare the results generated from the data to the results represented in the study. The viscoelastic properties were then used to calculate the Ciavarella code as well as the new code. These data series were then transposed onto replications of the result graphs seen in the Persson study. The results of that process can be seen in figure 3-2 and figure 3-3.
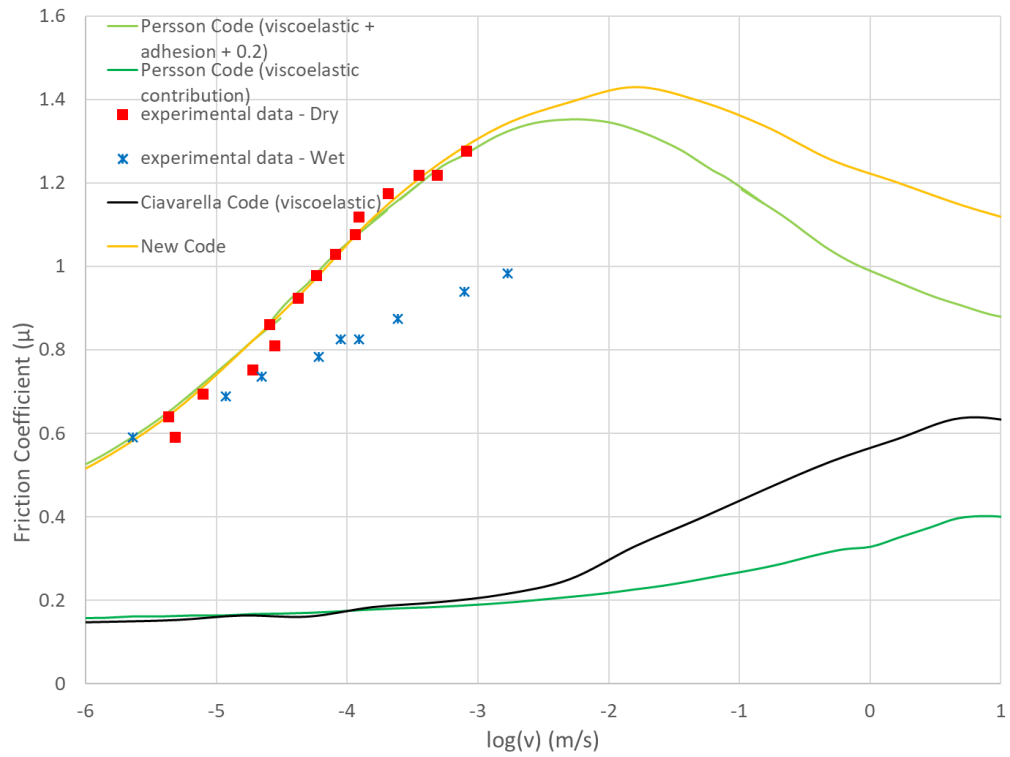
Figure **3-2**: The figure depicts the results from [39] for specimen B with the addition of the Ciavarella code and the new code.

Note: This figure was adapted from Tolpekina, T. V., and B N. J. Persson. "Adhesion and Friction for Three Tire Tread Compounds." *An Open Access Journal from MDPI*, Apollo Tyres Global R&D, 26 Feb. 2019, www.mdpi.com/journal/lubricants.
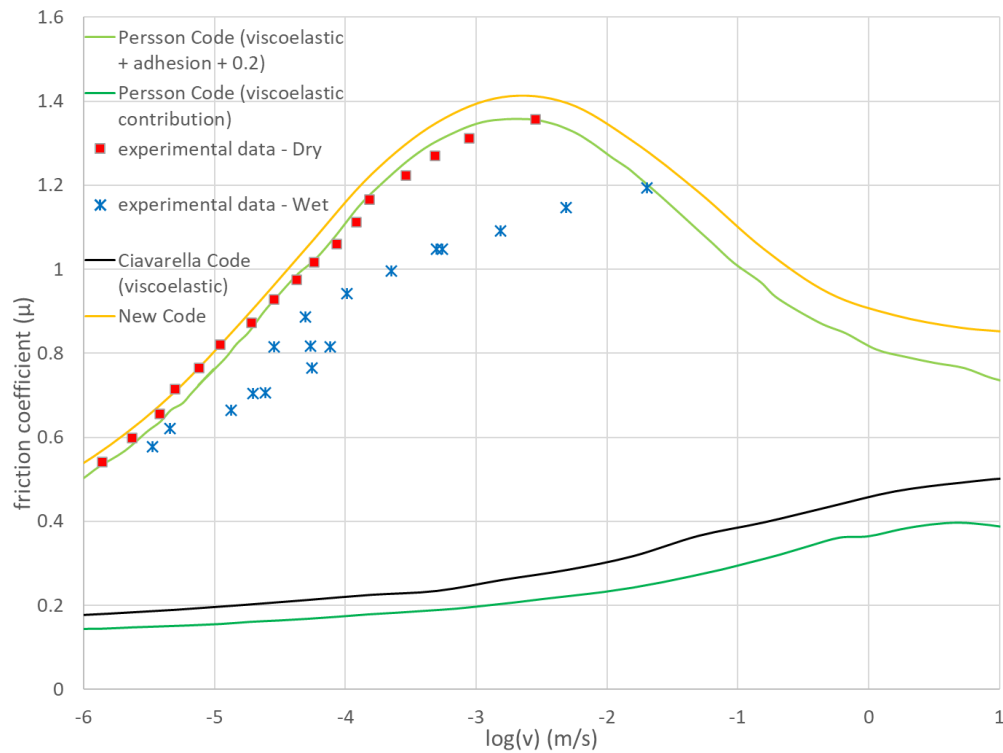
Figure **3-3**: The figure depicts the results from [39] for specimen C with the addition of the Ciavarella code and the new code.
Note: This figure was adapted from Tolpekina, T. V., and B N. J. Persson. "Adhesion and Friction for Three Tire Tread Compounds." *An Open Access Journal from MDPI*, Apollo Tyres Global R&D, 26 Feb. 2019, www.mdpi.com/journal/lubricants.

This provides good evidence for validation of the new code to match Persson's code and correlate with the experimental data. As the graphs depict, the new code correlates very well with the results of the study. The correlation is more apparent in figure 3-2 than figure 3-3, but the new code tends to give a higher value for the friction coefficient when considering higher sliding velocities. An error % was calculated in order to get a quantitative representation of the variance of the new code. The error % was calculated for the new code vs. the dry experimental data and for the new code vs the code for the total friction coefficient from Persson. This calculation was performed across the full frequency of the results, and all the data points from the original manipulation of

data. The process for data exportation, extrapolation, and calculation of the friction coefficient had to be repeated to correspond with the experimental data. Once this was completed, the error results could be calculated. The results can be seen in table 3-1.

3.3.2 Validation results

Table **3-1**: Validation results

Comparison between New Code and data from Tolpekina and Persson		
	% Error	
Specimen	**New Code vs Experimental data (dry)**	**New Code vs Calculation of total friction coefficient**
B	2.91	0.68
C	3.96	4.69
Average between specimens	3.44	2.69

The new code tracks closely to both Persson's code as well as the experimental data. The error was analyzed across the sliding velocities corresponding to the raw data from the experiments. This range is roughly log(-6) to log(-3) m/s. The equation used to calculate the percent error is as follows.

$$Error \ \% = abs(100 \times \frac{approximate - exact}{exact})$$

(20)

In equation (20), abs refers to the absolute value. In the place of approximate, the friction coefficient values from the new code were used. The values against which the new code was compared were the considered the "exact" values in that equation. In this instance, those values were the friction coefficient values from the Persson code and the

experimental friction results. For the results shown in table 3-1, at each data point the error % was calculated between the new code and the relevant curve. The absolute values of these errors were then summed and averaged to account for any error results that may have offset each other. An example would be one data point providing an error of +5% and another providing an error of –5%. Without taking the absolute value, these two would cancel each other out and the error would appear to be 0. For both specimens, B and C, the error % was less than 5% when compared to either the Persson code or the experimental data from the dry tests. This shows a very strong correlation and validates the accuracy of the new code. With multiple data sets to compare to, the validity of the new code is verified.
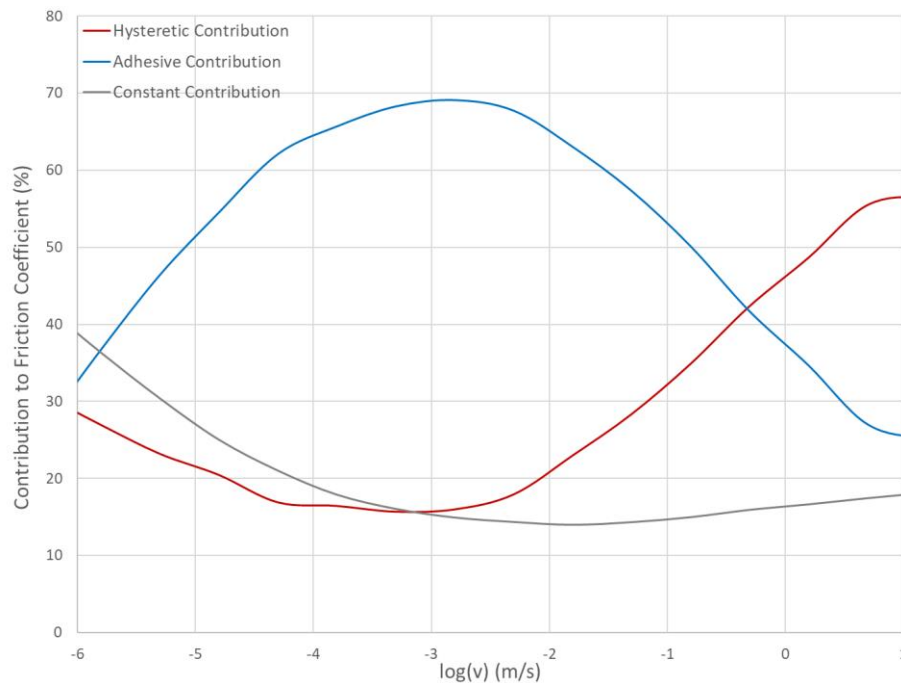
Figure **3-4**: The figure depicts the relative power of the hysteretic contribution to friction, adhesive contribution to friction, and the friction constant for the determination of the total friction coefficient in the new code

In this section the research on the simplification of the calculation of the hysteretic contribution to friction has been expanded by confirming its validity against additional data sets. A new code for the total friction coefficient has been developed by combining the simplified calculation for the hysteretic coefficient with the adhesive contribution of friction. Figure 3-4 shows the relative power of the contributions to friction for the new code across the frequency range. The new code reduces the calculations necessary for determining the hysteretic coefficient of friction to a simple 3 term multiplication. This study is continued with a parametric analysis and then investigates the use of direct testing data inputs on the result of the code.

IV CHAPTER

RESULTS AND DISCUSSION

4.1 Parametric Analysis

4.1.1   Selection of parameters

This study sought to determine what factors affect the friction coefficient and

which of these factors is most influential in altering the results of the model. As

established earlier in this paper, the friction coefficient is the result of complicated

physical reactions and events. Persson and other predominant researchers in the field of

rubber friction analysis consider a variety of factors: the viscoelastic properties of the

material, analysis of the surface roughness, ratio of real contact with the rubber to the

surface, the frictional shear stress generated, consideration for the level of magnification,

and the sliding velocity the specimen. All of these factors affect the calculations and

understanding which of these factors have the strongest influence on the calculation of

the coefficient of friction. This knowledge can indicate which areas of research can be

improved upon, in turn improving the model.

In order to analyze which factors have the most effect on the new code, a

parametric analysis was conducted. A parametric analysis measures the sensitivity of the

result to the variables of an equation. In this application, the final result is the friction

coefficient. One method for conducting a parametric study is to incrementally adjust eachof the variables and record the difference in the result. For this study, the parametric analysis was conducted by incrementally adjusting each of the variables and recording the difference in the result. The increments were set to 5%. Only the variable being analyze was adjusted, and all the other parameters were held constant. The percentage of change from the original data vs the parametric analysis was calculated and presented in table 4-1. Figure 4-1 shows the inputs used to conduct the parametric analysis. These values are from specimen B and were used to conduct the standard conditions seen in the parametric analysis.

Five different parameters were chosen to be analyzed when considering the friction coefficient calculated from the new code: The storage modulus, the loss modulus, the h'_{rms} of the surface, the selection of the wavelength cutoff number, and the adhesive contribution to friction. The storage modulus, or the elastic response of the material, and the loss modulus, or the viscous response of the material, are determined with DMA testing. These material properties can be affected or altered by material, filler, and mixing sections or conditions. The h'_{rms} of the surface and the selection of the wavelength cutoff number both help demonstrate the effect of the surface on the predicted friction coefficient.
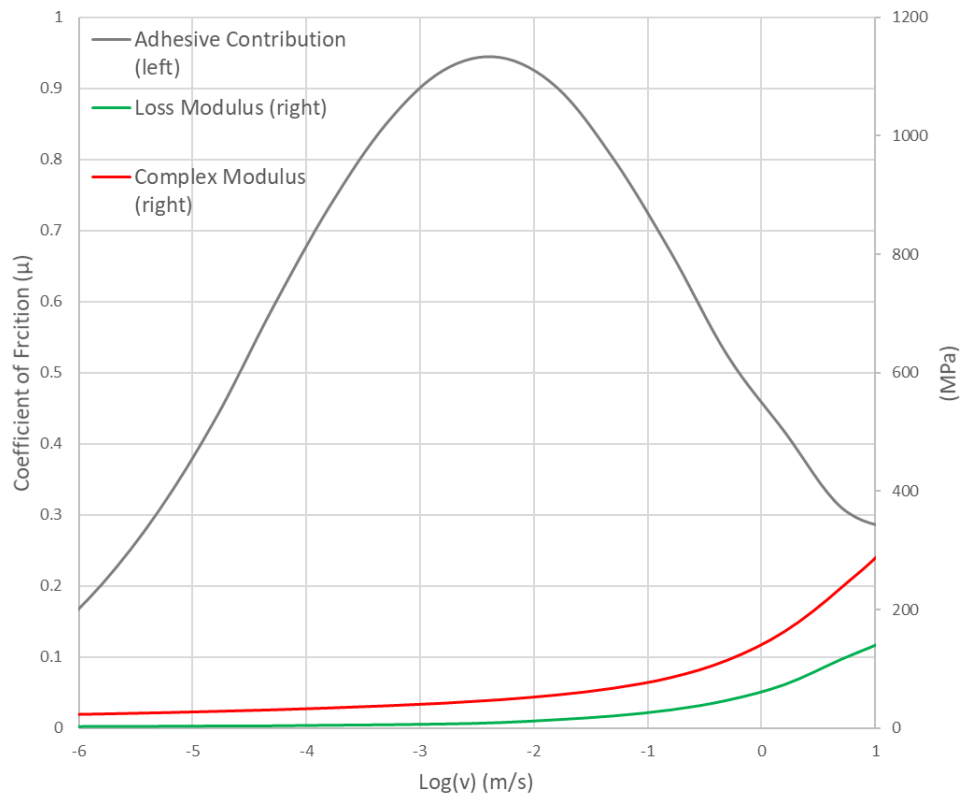
Figure **4-1**: Input parameters for the standard condition for the parametric analysis conducted in this study.

4.1.2 Storage modulus
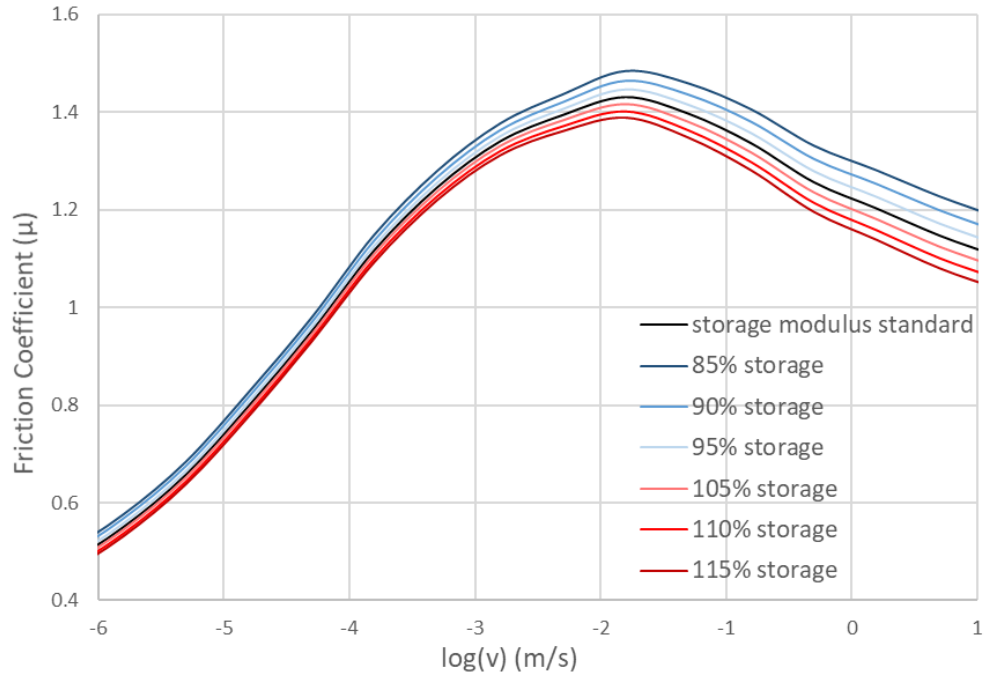
Figure **4-2**: The results of the parametric analysis of the storage modulus. The input parameters used for the standard condition can be seen in figure 4-1.

As seen in figure 4-2, the variation of the storage modulus, which is a material property, influences the friction coefficient. Because the storage modulus is in the calculation for the complex modulus changing the storage modulus affects the calculated friction coefficient. As discussed in the introduction of this study, the storage modulus is assigned as the real portion of the complex modulus. In equation (19), the storage modulus is incorporated into the denominator of the first term. The results of the analysis make sense mathematically, as one would expect that increasing the storage modulus would in turn decrease the generated friction coefficient. Similarly, decreasing the storage modulus increased the result for friction.

4.1.3 Loss modulus
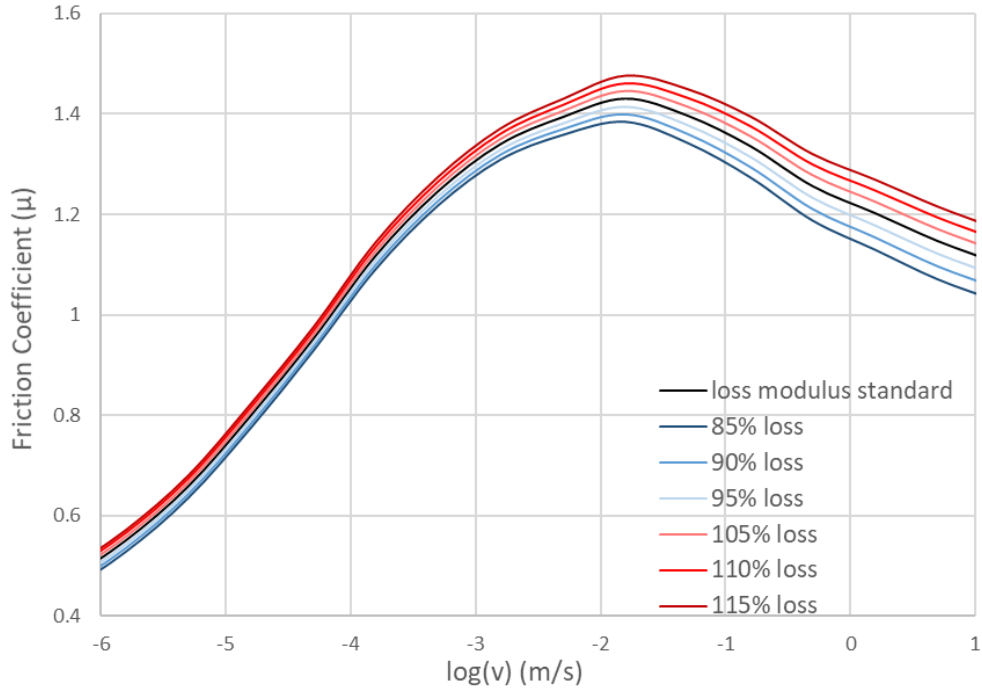
Figure **4-3**: The results of the parametric analysis of the loss modulus. The input parameters used for the standard condition can be seen in figure 4-1.

Unlike the storage modulus, the loss modulus can be directly seen in equation (19). The loss modulus, or viscous response of the material, is calculated alongside the storage modulus through DMA or similar testing. Based on the hysteretic contribution to friction in equation (19), it is clear that altering the loss modulus will modify the friction calculation proportionally. As the loss modulus is incrementally decreased, the calculated friction coefficient also decreases. When the loss modulus increases, the opposite occurs and the value for friction increases.

4.1.4 H'rms
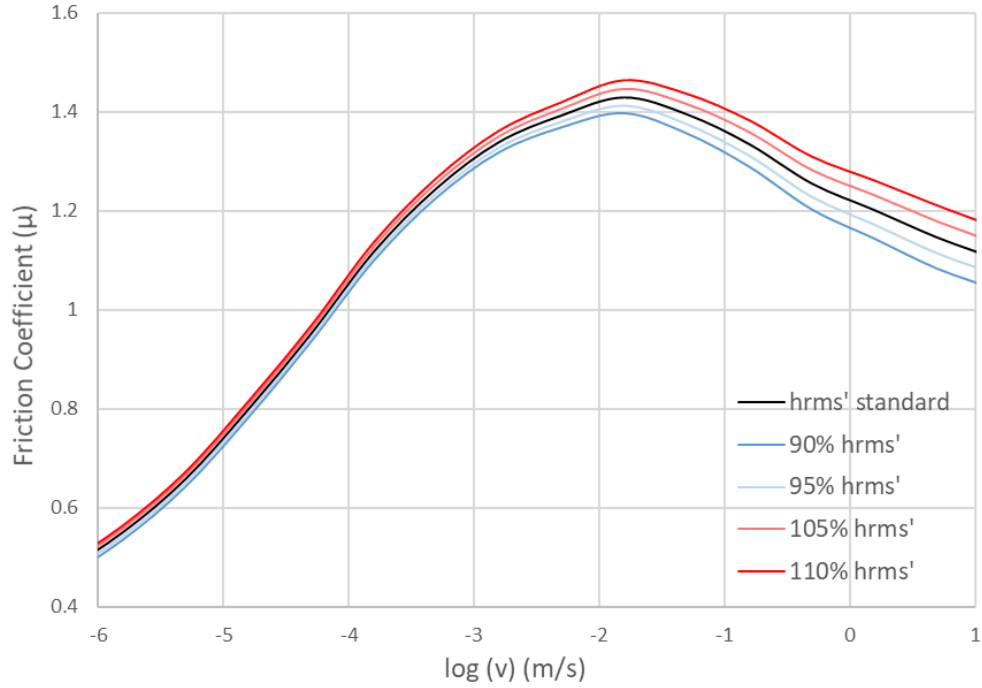
Figure **4-4**: The results of the parametric analysis of h'rms sensitivity. The standard h'rms of the application is valued at 1.3.

The adjustment of the h'rms is really an adjustment of the surface itself. Normally the h'rms is calculated through methods such as microscopy or other surface analysis techniques. In the new code, the h'rms is set to 1.3. However, by altering this value the calculated friction coefficient increases as the value of the h'rms increases. Likewise, a decrease in the h'rms will reverse the trend. This is apparent when viewing figure 4-4. The effect of this parameter is more pronounced at higher velocities. Which can be explained by the rise in the viscoelastic properties and the fall of the adhesive contribution in the higher frequency range.

4.1.5   Wavenumber cutoff
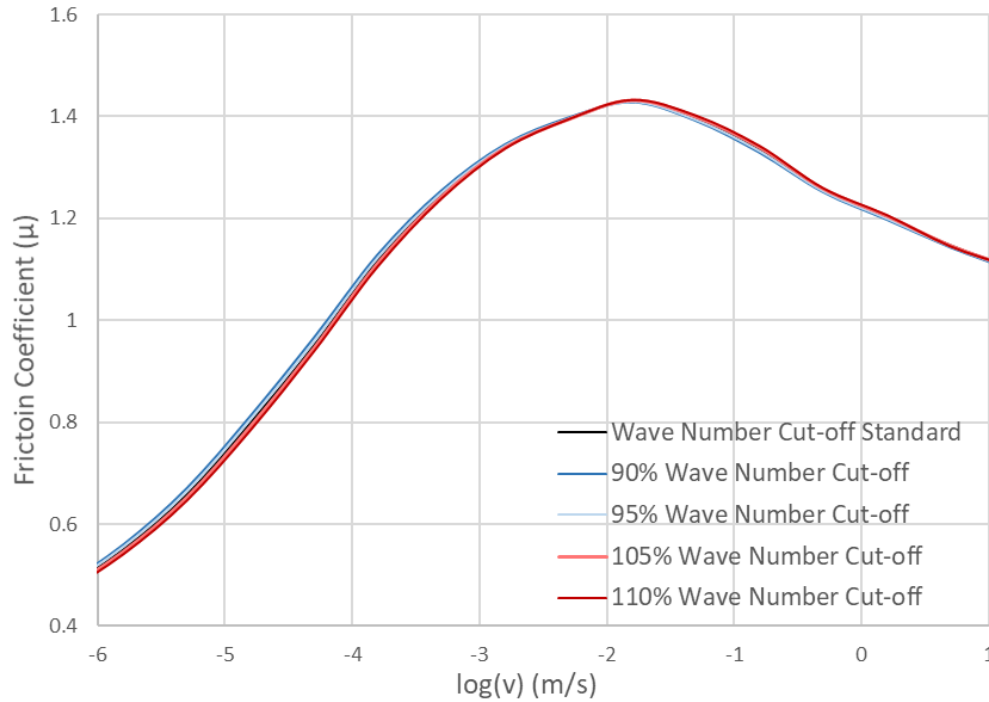
Figure **4-5**: The results of the parametric analysis of the wavenumber cutoff shown above. The standard value of the wavenumber is 2,000,000.

The wave number cut off is the selection that determines the end range of magnification to be considered in the surface analysis. Here the goal is to select limits to keep within the linear portion of the log(Cq), with C(q) being the power spectrum of surface roughness [37]. The real-world application of this selection theoretically affects the degree to which the rubber will deform while sliding across the surface. This deformation differs for each magnification level [37]. In figure 4-5, however, one can observe that varying this input has relatively little effect on the calculated friction coefficient when compared to the other parameters chosen. With less than 1% difference for any of the increments, the change of this parameter is a negligible amount.

4.1.6 Adhesive friction contribution
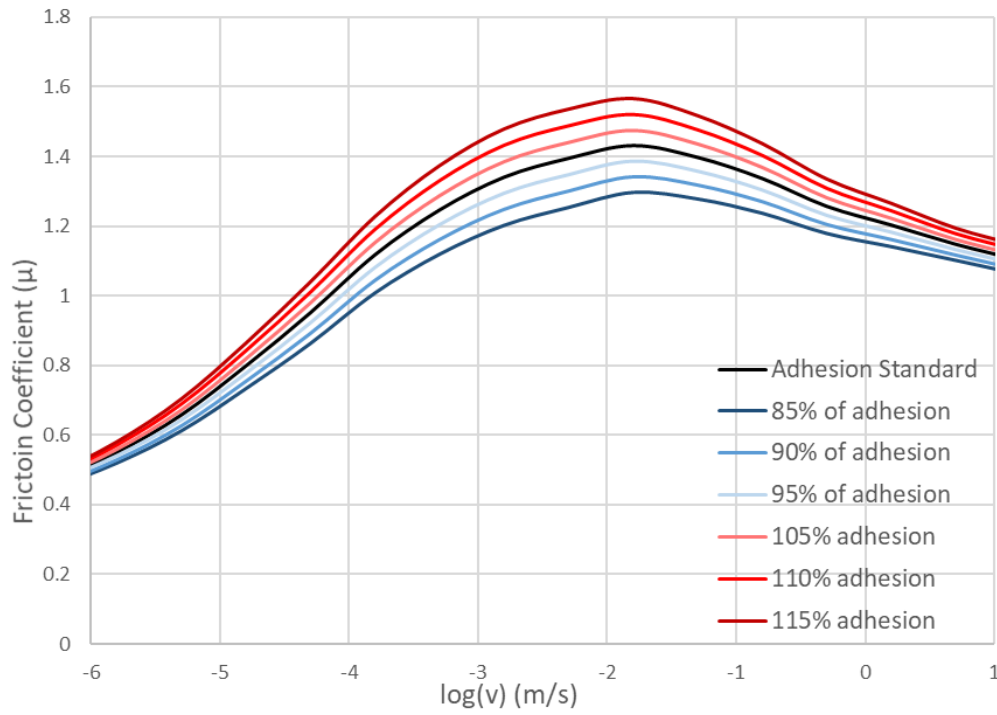
Figure **4-6**: The results of the parametric analysis of the adhesive contribution to the friction coefficient. The input parameters used for the standard condition can be seen in figure 4-1.

In figure 4-6, the parameter altered was the overall adhesive contribution. The calculation for the adhesive contribution to friction is seen in equations (16,17,18). The implementation of this analysis is straight forward. If the adhesive contribution is increased or decreased, the friction coefficient will respond accordingly. From the results shown above, the adhesive contribution plays a large role in determining the friction coefficient. When considering any potential simplifications for the adhesive contribution, care must be taken due to the influence it has on the results.

4.1.7   Parameter sensitivity

Table **4-1:** Parametric analysis results

Average Change for Parametric Analysis (%)						
Parameter	85%	90%	95%	105%	110%	115%
Storage Modulus	5.32	3.38	1.62	-1.48	-2.85	-4.12
Storage Modulus (abs)	5.32	3.38	1.62	1.48	2.85	4.12
Loss Modulus	-4.75	-3.14	-1.56	1.54	3.05	4.54
Loss Modulus (abs)	4.75	3.14	1.56	1.54	3.05	4.54
Adhesive Contribution	-6.01	-4.01	-2.00	2.00	4.01	6.01
Adhesive Contribution (abs)	6.01	4.01	2.00	2.00	4.01	6.01
h'_{rms}	-	-3.41	-1.68	1.78	3.51	-
h'_{rms} (abs)	-	3.41	1.68	1.78	3.51	-
Wave Number cut-off	-	0.27	0.13	-0.13	-0.26	-
Wave Number cut-off (abs)	-	0.92	0.45	0.41	0.79	-

Table 4-1 was constructed in the same manner as Table 3-1. Table 4-1 shows the

parametric analysis and the calculated percentage change from the standard variable

condition to each of the adjusted conditions. For this calculation, the error % equation

(20) was used to determine these results. For each parameter, the percent change was

calculated at each data point and then averaged across the range of data. For the analysis,

the actual error and the absolute value of the error at each data point have both been

calculated. The reason for this was to account for potentially offsetting positive and

negative changes.

The analysis demonstrates the new codes' sensitivity to each of the input variables and conditions. The study shows that the strength that the parameters had on the friction varied greatly. These effects ranged from 0.13% to 6.01%. The weakest of the parameters was the wave number cutoff selection. A 0.92% increase in the friction coefficient, when the wave number cutoff was 180,000 or 90% of its original value, was the largest average affect attributed to this parameter. This result aids Ciavarella's claims that the wave number cutoff is an insignificant consideration for the calculation of the friction coefficient.

The viscoelastic properties were determined to be very important input parameters for the coefficient of friction. This is clear in the results of the storage and loss moduli, which contributed to maximum averaged changes of 5.32% and 4.12% respectively. Another important parameter was the adhesive contribution to friction. The largest change from this parameter was seen at the two extremes, resulting in 6.01% shift in the friction coefficient. The new code is most sensitive to changes in the loss modulus, storage modulus, and the adhesive contribution to friction. These results demonstrate that a precise determination of the viscoelastic properties of a compound is a major factor in an accurate prediction of the friction coefficient.

4.2 Performance indicators and selected frequencies

Ever since John Boyd Dunlop patented the pneumatic tire in 1888, tires have been evolving, and tire manufacturers are constantly striving to create tires that perform well in a variety of applications. Today, the tire industry sells 100 billion units worldwide every year, and the market is valued around one tenth of a trillion dollars [7]. The purpose of

the tire is to keep the driver in control of the vehicle by supporting the vehicle and transferring the power generated by the engine to the pavement. Construction equipment, sports utility vehicles, light trucks, and passenger vehicles have unique needs – or performance indicators – when it comes tire performance and function. The most investigated performance indicators for tires are wet traction, dry handling and traction, rolling resistance, and snow and ice traction. Wear resistance is another important attribute for all tires.

For passenger tires, the most important performance areas are wet traction and rolling resistance. Tires need to maintain healthy traction on all types of road conditions, and low rolling resistance is crucial for improving the fuel economy of the car. When it comes to tire tread, there are many performance tradeoffs to consider. For example, a harder compound will allow for better rolling resistance and increased wear resistance, but it will generally result in less favorable numbers for parameters such as wet traction [7]. Tire manufacturers commonly use DMA to gauge these parameters. Utilizing DMA allows tire manufacturers and engineers to map these performance predictors to specific regions of the master curve for the material [12]. The following sections will discuss the frequencies and the DMA indicators that relate to the performance parameters.

4.2.1   Wet traction

Wet traction refers to driving conditions in which the road surface is wet. Real-world experience and numerous experiments have shown that a wet surface produces a lower friction coefficient than a dry surface [37, 39]. Experimental results can be seen in figures 3-2 and 3-3. Water on a road surface affects the texture of the surface by filling in

some of the valleys of the pavement corrugations [7]. When the vehicle reaches a particular speed, the area of real contact between the rubber and the substrate will become separated by a thin film of fluid. In these conditions, the adhesive contribution is reduced, and the hysteretic contribution dominates the friction coefficient [23]. The DMA performance predictors for wet traction are the loss modulus and, in turn, tan(δ). When conducting a DMA analysis on a tire tread, the region that relates to wet traction is 0°C [12]. Different manufacturers may shift this value slightly, but the tan(δ) at 0°C is an indicator of the rubber's proficiency in wet traction. The wet traction of the material increases as tan(δ) increases.

4.2.2   Dry handling/traction

Traction and handling are critical performance areas for performance vehicles that also impact everyday drivers. These functions are essential for vehicle operation. Dry handling is predicted by comparing a material's storage modulus and complex modulus. Loss compliance is the viscoelastic property that indicates dry traction performance. In both instances, as these parameters increase, the corresponding performance indicator increases. The indication temperature for both parameters is 30°C [12]. The intended operation of the tire and vehicle determines the relative importance of each of these areas of performance.

4.2.3   Rolling resistance

Rolling resistance is one of the most relevant parameters for civilian automobilists. As the rolling resistance of a tire decreases, the fuel economy for the

vehicle increases. This lowers the economic imprint of the vehicle and saves money for the consumer. The simplest way to visualize this parameter is via the Maxwell model of the spring and dashpot. Low rolling resistance would indicate that the tread material acts like a spring storing energy and allowing the tire to rebound off the road. If the tire tread shows high rolling resistance, the tread performs more like a dash pot, taking in the energy and dissipating it. The viscoelastic property generally associated with rolling resistance is $\tan(\delta)$, and the associated temperature is 60°C. If the $\tan(\delta)$ increases, the rolling resistance will also increase. In this instance, the increase in rolling resistance results in a negative impact on the performance.

4.2.4 Snow/ice traction

Snow and ice traction are both measured with DMA at temperatures of -15°C and -10°C, respectively. Measuring the storage modulus in tension is one method to determine the performance of tire tread for snow traction [12]. Drivers in the northern United States regularly experience winter driving conditions and the traffic slowdowns that often come with snow and ice. Under these dangerous driving conditions, it is of paramount importance that the tires maintain friction and keep the driver in control of the vehicle. Having a strong indicator of how a tire will perform under these conditions helps manufacturers develop better products for applications such as this. Using DMA, snow and ice traction can be predicted using the complex and storage moduli for snow traction and the $\tan(\delta)$ and loss modulus for ice traction. Snow traction will improve with lower values of the storage and complex modulus. Similarly, ice traction improves for higher values of the $\tan(\delta)$ and loss modulus.

4.2.5   Calculation of frequencies for performance predictors

Tire manufacturers utilize DMA data to compare the performance indicators of their own products with competitor products. This process includes DMA testing and comparing the relative viscoelastic properties of various tires at the target temperatures. This comparison shows how a tire will perform in one application relative to another tire, allowing researchers and manufacturers to rank tires in order of their performance predictors.

In order to determine the frequency ranges seen in table 4-2, information from specimen B of the Tolpekina and Persson study was used [39]. In the study, the team used the WLF equation to determine the shift factor for tread specimen B across a large temperature range. In order to pull out the appropriate values for the target temperature range, the Webplot Digitizer app was used to reproduce the data points. Generic DMA test conditions were assumed in order to develop table 4-2. The frequency for testing can vary from test to test and company to company. In general, test frequency can be chosen between 1 Hz and 100 Hz. For this study, a DMA test frequency of 1 Hz was chosen. To account for the variability between companies' chosen prediction temperatures or test frequencies, a range was created by taking ± 5°C of the standard indication temperatures. The shift factor was taken from the WLF information in [39] and applied at each of the temperature points. Table 4-2 shows the target temperature and range, the master curve frequency range, the relative viscoelastic property, and the effect the viscoelastic property has on the performance factor for each performance factor.

Table **4-2:** Tire performance indicators

Tire Performance Factor	Temperature Target/range (°C)	Corresponding Master Curve Frequency Range (Hz)	Corresponding Viscoelastic Properties	Effect of Viscoelastic Property on Tire Performance Factor
Wet Traction	0 / -5 to 5	300 to 7,300	Loss Modulus and Tan(δ)	Factor improves as the viscoelastic property increases.
Dry Traction	30 / 25 to 35	no shift	Loss Compliance	Factor improves as the viscoelastic property increases.
Dry handling (cornering)	30 / 25 to 35	no shift	Complex Modulus and Storage Modulus	Factor improves as the viscoelastic property increases.
Rolling Resistance	60 / 55 to 65	no shift	Tan(δ)	Factor improves as the viscoelastic property decreases.
Snow Traction	-15 / -10 to -20	38000 to 1,544,400	Complex Modulus and Storage Modulus	Factor improves as the viscoelastic property decreases.
Ice traction	-10 / -15 to -5	7,300 to 230,000	Tan(δ) and Loss Modulus	Factor improves as the viscoelastic property increases.

4.3 Incorporation of HFDMA

4.3.1 Study results

Testing at higher frequencies allows for a more direct and more consistent representation of the conditions that rubber will experience in the real world. In the study developed by Esmaeeli in 2019, a new high frequency DMA was developed. The

objective was to demonstrate more accurately the response of tire tread rubber from actual driving conditions. As previously stated, direct testing of the rubber specimen would help mitigate some of the disadvantages of using the WLF method. Utilizing this direct testing would allow better representation of thermorheologically complex polymers. In the following sections testing data from Esmaeeli and Farhad, see Table-3, is used and extrapolated to analyze how it affects the calculation for the coefficient of friction. This data is also used to investigate the differences between HFDMA and DMA, using the WLF shift equation, for the tire performance predictors at the target temperature points.

Table **4-3:** DMA and HFDMA testing results from Esmaeeli and Farhad

DMA and HFDMA Test Data for a Carbon Black filled Rubber								
Frequency	DMA data				HFDMA data			
	G'	G''	tanδ	G*	G'	G''	tanδ	G*
100	1.00E+07	2.11E+06	0.211	1.02E+07	1.01E+07	2.12E+06	0.212	1.03E+07
160	1.04E+07	2.21E+06	0.214	1.06E+07	1.04E+07	2.23E+06	0.214	1.07E+07
250	1.10E+07	2.40E+06	0.218	1.13E+07	1.11E+07	2.47E+06	0.22	1.14E+07
400	1.15E+07	2.50E+06	0.218	1.17E+07	1.17E+07	2.58E+06	0.22	1.20E+07
1000	1.25E+07	2.77E+06	0.222	1.28E+07	1.30E+07	2.93E+06	0.225	1.33E+07
1600	1.30E+07	2.94E+06	0.226	1.33E+07	1.35E+07	3.15E+06	0.231	1.38E+07
2100	1.35E+07	3.11E+06	0.230	1.39E+07	1.41E+07	3.39E+06	0.239	1.45E+07
3800	1.41E+07	3.29E+06	0.233	1.45E+07	1.48E+07	3.32E+06	0.245	1.51E+07
5000	1.48E+07	3.52E+06	0.238	1.52E+07	1.57E+07	3.56E+06	0.253	1.61E+07
DMA and HFDMA Test Data for a Silica filled Rubber								
Frequency	DMA data				HFDMA data			
	G'	G''	Tan(δ)	G*	G'	G''	Tan(δ)	G*
100	6.99E+06	2.49E+06	0.356	7.43E+06	7.05E+06	2.50E+06	0.36	7.48E+06
160	7.38E+06	2.78E+06	0.377	7.89E+06	7.45E+06	2.79E+06	0.38	7.95E+06
250	7.95E+06	3.22E+06	0.405	8.58E+06	8.07E+06	3.25E+06	0.41	8.70E+06
400	8.70E+06	3.87E+06	0.445	9.52E+06	8.86E+06	3.92E+06	0.45	9.69E+06
1000	1.07E+07	5.79E+06	0.541	1.22E+07	1.10E+07	5.90E+06	0.55	1.25E+07
1600	1.19E+07	7.06E+06	0.593	1.38E+07	1.24E+07	7.24E+06	0.61	1.44E+07
2100	1.30E+07	8.28E+06	0.638	1.54E+07	1.36E+07	8.60E+06	0.67	1.61E+07
3800	1.57E+07	1.16E+07	0.735	1.95E+07	1.66E+07	1.21E+07	0.77	2.06E+07
5000	1.83E+07	1.46E+07	0.800	2.34E+07	1.95E+07	1.54E+07	0.85	2.48E+07

Looking at the data, the values for DMA and HFDMA were similar at frequencies under 1000 Hz. The differences between DMA and HFDMA data start to become apparent above 1000 Hz. This could be due to the fact that the DMA utilizes the WLF shift equation. It is also important to note that these changes have stronger potential to affect wet, snow, and ice traction, as the target frequency ranges are above 1000 Hz. Using the supplied data, the percentage difference between the viscoelastic parameters was calculated for each of the frequencies shown. A linear extrapolation was then performed on the data to find the results at the target frequencies for the tire performance parameters, seen in table 4-5. This procedure was also used to calculate the percent changes for each of the viscoelastic parameters across the frequency range used to present the results for the calculations of the coefficient of friction. The differences from HFDMA where then applied to the input values for the coefficient of friction, and the new code with the HFDMA adjustments was calculated, as seen in figure 4-7 and figure 4-8. Specimen B is a carbon black-filled tire tread, and Specimen C is a silica-filled tread. The HFDMA results were applied accordingly. One major assumption made in this calculation was that the HFDMA results directly translated from one material to another. This was a necessary simplification in order to utilize the available data. There are still too many unknowns to claim that the HFDMA results can be directly translated simply because of the same filler type.

4.3.2 Effect on coefficient of friction

Figure **4-7**: The new code for coefficient of friction for specimen B from [39] plotted against the version of the code using updated input values from the HFDMA data.
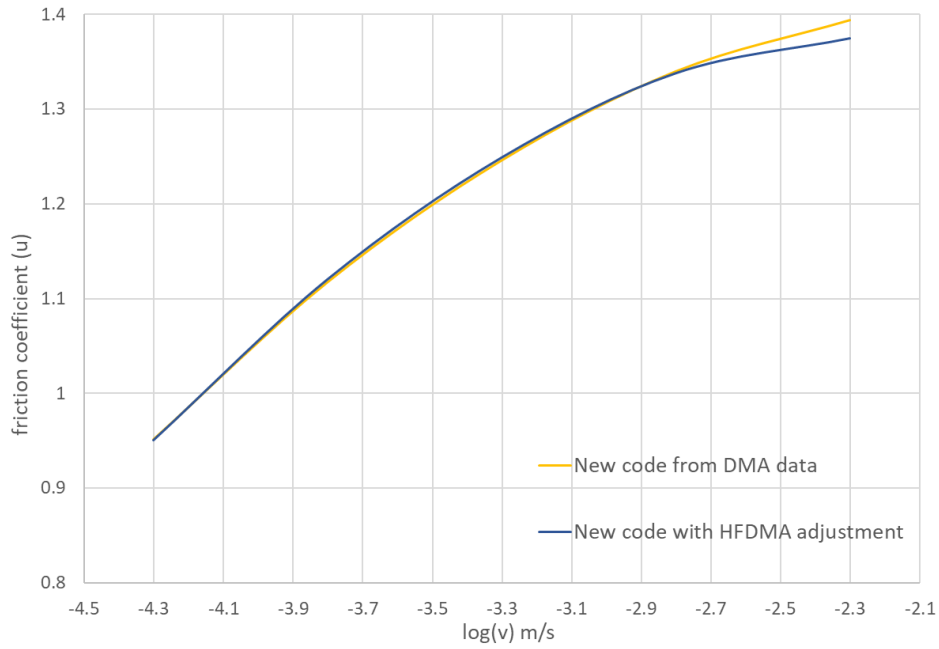

Figure **4-8**: The new code for coefficient of friction for specimen C from [39] plotted against the version of the code using updated input values from the HFDMA data.
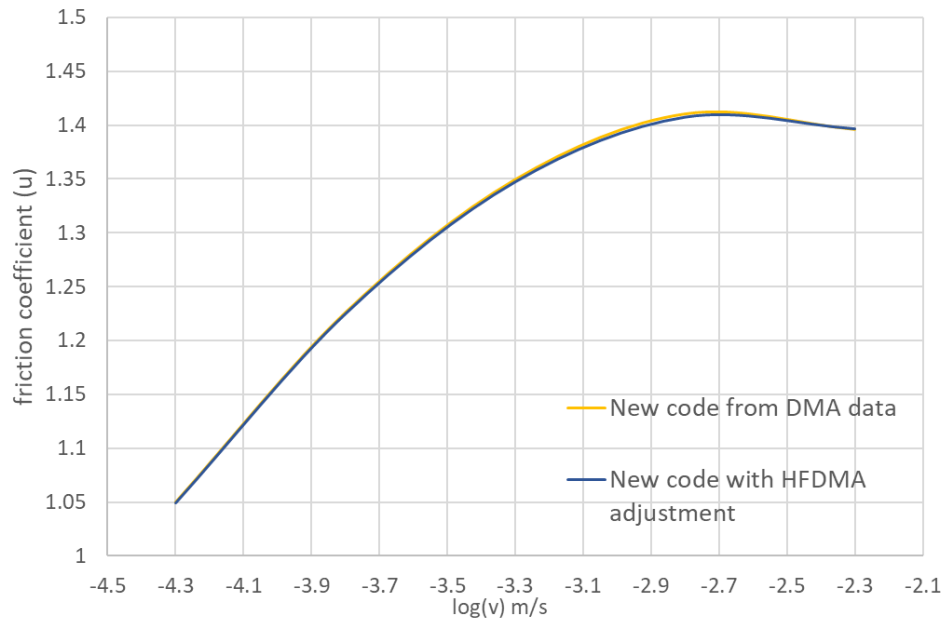
The results shown in figures 4-7 and 4-8 demonstrate that the change in input parameters from the HFDMA data has a negligible effect on the coefficient of friction in the range of sliding velocity of log(-4.5) to log(-2.3). This result makes sense since the average percentage change between the parameters is around 1% within the range shown in the two figures. From the HFDMA data, one can see that the major changes tend to occur at higher frequencies. In table 4-4, the % change from the original friction coefficient calculation to the HFDMA updated results is represented.

The maximum overall change is seen at log(-2.3) with a % change of -1.36%. At all other calculated frequencies, the change was less than 1%. For the best understanding of the real effect of the HFDMA, the HFDMA testing would need to be conducted directly on specimens B and C.

Table **4-4:** Difference between DMA and HFDMA testing

% Change in Friction Coefficient from DMA data to HFDMA data			
Log(v) (m/s)	Hz	Specimen B	Specimen C
-4.30	100	-0.09	-0.09
-3.80	316	0.28	-0.10
-3.30	1000	0.26	-0.15
-2.80	3162	-0.12	-0.20
-2.30	10000	-1.36	0.06

4.3.3   Effect on tire performance indicators

The final area to analyze is the potential effect of the HFDMA on the determination of tire performance predictors. These predictors are pulled from DMA data to gain insight into how a given rubber material will perform in one of the applications of vehicle travel over roadways. As previously discussed, DMA testing utilizes the TTS by

conducting oscillatory testing during a temperature sweep. The aim of the HFDMA is to

improve the accuracy of the determination of the viscoelastic properties of a material.

This is achieved by direct measurement instead of relying on the WLF equation.

Table **4-5**: HFDMA effect on the tire performance indicators.

Results from HFDMA for different Rubber Compounds				
Rubber Composition	**Tire Performance Factor**	**Corresponding Viscoelastic Properties**	**% Change from DMA to HFDMA for Relevant Property**	**Predicted Effect on Performance Factor**
SBR	Wet Traction	Loss Modulus (E") and Tan(δ)	≈ 6% increase in Tan(δ)	Improved
	Snow Traction	Complex Modulus (E*) and Storage Modulus (E')	≈ 6% avg increase between E' and E*	Decreased
	Ice Traction	Loss Modulus (E") and Tan(δ)	≈ 6% increase in Tan(δ)	Improved
Carbon Black filled SBR	Wet Traction	Loss Modulus (E") and Tan(δ)	≈ 6.5% increase in Tan(δ)	Improved
	Snow Traction	Complex Modulus (E*) and Storage Modulus (E')	≈ 6.4% avg increase between E' and E*	Decreased
	Ice Traction	Loss Modulus (E") and Tan(δ)	≈ 6.5% increase in Tan(δ)	Improved
Silica filled SBR	Wet Traction	Loss Modulus (E") and Tan(δ)	≈ 6.25% increase in Tan(δ)	Improved
	Snow Traction	Complex Modulus (E*) and Storage Modulus (E')	≈ 6.3% avg increase between E' and E*	Decreased
	Ice Traction	Loss Modulus (E") and Tan(δ)	≈ 6.25% increase in Tan(δ)	Improved

Table 4-5 illustrates the effect that the results from the HFDMA have on the tire performance predictors. The parameters that will be affected by the HFDMA are wet, snow, and ice traction. The viscoelastic properties found or derived during DMA testing are used as indicators to predict tire performance. The table shows the rubber compounds and how each of the relative performance predictors are altered when considering the HFDMA data. For wet traction, $\tan(\delta)$ is the indicator parameter. For each of the compounds, the HFDMA showed an increase in $\tan(\delta)$, and the average increase was 6.25%. The increase in $\tan(\delta)$ translates to better performance in wet traction. When considering snow traction, both viscoelastic property indicators increased. The average property increase was 6.23% when averaged between the complex and storage modulus for each of the three compounds. This increase predicts a decreased level of performance regarding snow traction. The final parameter analyzed was ice traction. The loss modulus and $\tan(\delta)$ are used to compare how compounds will perform during icy road conditions. The average increase for $\tan(\delta)$ was already stated to be 6.25%. For ice traction, the increase in $\tan(\delta)$ also leads to improved performance for the application. It also important to note that the carbon black-filled SBR showed the largest increase between the viscoelastic properties when compared to the traditional DMA. Whether this was due to the filler choice, amount of filler, or level of dispersion is still up for debate.

V CHAPTER

CONCLUSION AND FUTURE WORKS

The tread is the primary component of the tire that translates the power from the engine to the pavement. The tire needs to maintain friction with the road surface for control during maneuvering. The challenge is finding the appropriate level of friction needed for control without increasing the rolling resistance to a degree that hinders the overall performance of the vehicle. For proper modelling of the tire, manufacturers must have the correct data on the rubber compounds and other components used. In many cases, the necessary data on the viscoelastic properties of the rubber is determined through DMA testing. These properties are extremely important for the prediction of a rubber tread's performance, as well as the determination of friction factor.

Tires are highly engineered products composed of six major components: tread, inner liner, sidewall, belts, body ply, and bead. Each of these components has a highly specific purpose and function and must be designed and developed properly to ensure overall function of the tire. There are many choices to make throughout the manufacturing process that will alter the properties of the material and the performance of the final component. The base material is usually chosen first, followed by the amount and type of filler, which can alter the hardness and elastic modulus of the rubber. Different oil additives and mixing plans can also alter the material properties of the compound.

After the compound is developed, material properties need to be verified in order to validate the modeling process and quality. DMA is used to generate the viscoelastic properties of the material, such as tan(δ) and the complex, storage, and loss moduli. Cyclic stressing in a laboratory setting gives manufacturers a high-level understanding of how the material absorbs and dissipates energy. This data is crucial for calculating the coefficient of friction.

A central focus of this study was to investigate methods for calculation of the coefficient of friction. I analyzed methods from multiple studies that investigated the friction coefficient and combined the equations from these studies to develop a new, simple code for determination of the coefficient of friction. The resulting new code can be seen in equation (19). This code was then validated against two additional data sets.

The analysis found a difference of 0.68% for the first data set and a difference of 4.69% between the new code and the second data set. With these results, the knowledge and data pertaining to the new code have been expanded. The close relation to the new code and the results from [39] allow us to determine that the new code is a suitable alternative to some of the methods being used to calculate rubber friction today.

To better understand this new code, a parametric analysis was conducted on five inputs: the wave number cutoff, h'_{rms}, the storage modulus, the loss modulus, and the adhesive contribution to friction. The parametric analysis found that the loss modulus, storage modulus, and adhesive contribution to friction had the strongest impact on the value of the coefficient of friction. The maximum effect was 4.75%, 5.32%, and 6.01% respectively. This reinforced the idea that the most important variables for the new code are the viscoelastic properties.

With results showing the significance of the viscoelastic properties, this study was continued with the introduction of the HFDMA data. The HFDMA measures viscoelastic properties of materials through direct testing as opposed to relying on the WLF shift equation. The effect of HFDMA testing on the coefficient of friction and on the effect on the tire performance predictors were analyzed. Based on the study, the effect of the HFDMA on the friction was miniscule. However, the results showed that the HFDMA affected the viscoelastic properties used as indicators for the wet, snow, and ice traction. The new results displayed an average change of 6% in these viscoelastic properties. The differences started to become apparent after the frequency point of 1,000 Hz. The study demonstrated the relevance of HFDMA data to predicting of tire performance.

This study achieved some progress in the study of rubber friction. A new code has been confirmed for the coefficient of friction, and the relevance of HFDMA testing has been established. However, this study only represents an initial investigation. There are many opportunities for future studies to expand upon these investigations and discoveries. One such opportunity would be to improve upon our understanding of the adhesive contribution to friction and use that knowledge to enhance the new code. In its current state, the code utilizes the adhesive contribution of friction in its full form. A better understanding and additional experimentation could enable the development of a simplified version of this input. A fully simplified code would cut down on the computational stress needed for friction analysis. Ideally, the new code would then be tested in order to verify that it maintains fidelity when applied to compounds with different filler levels and filler types.

This study could also be improved by conducting additional experimentation. In an ideal scenario, at least five different rubber tread compounds with varying levels of filler could be comprehensively tested and analyzed. A successful study would need enough sample tires to excise specimens from the tread for DMA, HDMA, and friction testing and whole tires to conduct force and moment testing. Force and moment testing machines would be utilized to measure cornering, rolling resistance, and braking performance. Additionally, whole tires could be mounted onto vehicles and driven at a winter test track to measure on-vehicle performance in real time.

This comprehensive testing program would generate a large pool of data that could then be used to cross-check many calculations and applications. With the friction testing data, an investigator could use the new code for coefficient of friction to compare the calculated results using the DMA and the HFDMA generated inputs against the experimental data. This would determine how the new code accommodates varying filler amounts and whether there is a significant difference between the DMA and HFDMA input values. This will also allow for some additional investigate of the friction coefficient, μ_{const}. The data generated from the HFDMA and DMA could then be used to predict the performance indicators for these tires. This will also allow for some additional investigate of the friction coefficient, μ_{const}. With data gathered from force and moment and on-vehicle testing, researchers would be able to directly investigate the power of the HFDMA for rubber analysis. With this additional data, the code for calculation of the friction coefficient can be further developed. With further development the adhesive contribution can be simplified, and an equation could be developed for the friction constant, μ_{const}. Eventually a code could be developed to incorporate all the

contributions to the coefficient of friction into one calculation. I will leave this

advancement to future studies. This is an ever-growing industry and every bit of

knowledge unlocked helps propel the field forward.

BIBLIOGRAPHY

[1]   Association of Rubber Products Manufacturers (2019) "Technical Guidance Document for State of Cure". Sp-913, Association for Rubber Products Manufacturers, Indianapolis, IN. Available at www.arpminc.com

[2]   Carbone, G., and C. Putignano. "Rough Viscoelastic Sliding Contact: Theory and Experiments." *Physical Review E*, vol. 89, no. 3, 2014, doi:10.1103/physreve.89.032408.

[3]   Chang, Xiang-dong, et al. "Experimental Investigation on the Characteristics of Tire Wear Particles under Different Non-Vehicle Operating Parameters." *Tribology International*, vol. 150, 2020, p. 106354., doi:10.1016/j.triboint.2020.106354.

[4]   Chernyak, Yu.B., and A.I. Leonov. "On the Theory of the Adhesive Friction of Elastomers." *Wear*, vol. 108, no. 2, 1986, pp. 105–138., doi:10.1016/0043-1648(86)90092-x.

[5]   Ciavarella, M. "A Simplified Version of Persson's Multiscale Theory for Rubber Friction Due to Viscoelastic Losses." *Journal of Tribology*, vol. 140, no. 1, 2017, doi:10.1115/1.4036917.

[6]   Dick, John, and Karl Winkler. "Understanding Dynamic Properties of Rubber and Rubber Products." Akron Polymer Training Center. 2018, Akron, The University of Akron.

[7]   Esmaeeli, Roja. "DIRECT TESTING OF TIRE TREAD COMPOUNDS AT HIGH FREQUENCIES USING A NEWLY DEVELOPED DYNAMIC MECHANICAL ANALYSIS (DMA) SYSTEM." *The University of Akron*, 2020.

[8]   Geethamma, V. G., et al. "Vibration and Sound Damping in Polymers." *Resonance*, vol. 19, no. 9, 2014, pp. 821–833., doi:10.1007/s12045-014-0091-1.

[9]   Greenwood, J A. "The Theory of Viscoelastic Crack Propagation and Healing." *Journal of Physics D: Applied Physics*, vol. 37, no. 18, 2004, pp. 2557–2569., doi:10.1088/0022-3727/37/18/011.

[10]   Grosch, K A. "The Relation between the Friction and Visco-Elastic Properties of Rubber." *Proceedings of the Royal Society of London. Series A. Mathematical and Physical Sciences*, vol. 274, no. 1356, 1963, pp. 21–39., doi:10.1098/rspa.1963.0112.

[11]   Grosch, K. A. "The Rolling Resistance, Wear and Traction Properties of Tread Compounds." *Rubber Chemistry and Technology*, vol. 69, no. 3, 1996, pp. 495–568., doi:10.5254/1.3538383.

[12]   Flanigan, Cynthia M, et al. "SUSTAINABLE PROCESSING OILS IN LOW RR TREAD COMPOUNDS." *Rubber News*, Ford Motor Company, www.rubbernews.com/assets/PDF/RN86691218.pdf.

[13]   Heinrich, Gert. "Hysteresis Friction of Sliding Rubbers on Rough and Fractal Surfaces." *Rubber Chemistry and Technology*, vol. 70, no. 1, 1997, pp. 1–14., doi:10.5254/1.3538415.

[14]   Heinrich, Gert, and Manfred Klüppel. "Rubber Friction, Tread Deformation and Tire Traction." *Wear*, vol. 265, no. 7-8, 2008, pp. 1052–1060., doi:10.1016/j.wear.2008.02.016.

[15]   Johnson, K. L., and J. A. Greenwood. "Adhesion of Viscoelastic Spherical Solids." *Solid Mechanics and Its Applications*, 2002, pp. 141–160., doi:10.1007/978-94-017-1154-8_16.

[16]   Kaewsakul, W., et al. "OPTIMIZATION OF MIXING CONDITIONS FOR SILICA-REINFORCED NATURAL RUBBER TIRE TREAD COMPOUNDS." *Rubber Chemistry and Technology*, vol. 85, no. 2, 2012, pp. 277–294., doi:10.5254/rct.12.88935.

[17]   Klüppel Manfred, and Gert Heinrich. "Rubber Friction on Self-Affine Road Tracks." *Rubber Chemistry and Technology*, vol. 73, no. 4, 2000, pp. 578–606., doi:10.5254/1.3547607.

[18]   Lyashenko, I. A., et al. "Comment on 'Friction Between a Viscoelastic Body and a Rigid Surface with Random Self-Affine Roughness.'" *Physical Review Letters*, vol. 111, no. 18, 2013, doi:10.1103/physrevlett.111.189401.

[19]   Le Gal, André, et al. "Evaluation of Sliding Friction and Contact Mechanics of Elastomers Based on Dynamic-Mechanical Analysis." *The Journal of Chemical Physics*, vol. 123, no. 1, 2005, p. 014704., doi:10.1063/1.1943410.

[20]   Ljubic, Darko, et al. "Time: Temperature Superposition Principle: Application of WLF Equation in Polymer Analysis and Composites." *Zastita Materijala*, vol. 55, no. 4, 2014, pp. 395–400., doi:10.5937/zasmat1404395l.

[21] Lorenz, B., et al. "Rubber Friction: Comparison of Theory with Experiment." *The European Physical Journal E*, vol. 34, no. 12, 2011, doi:10.1140/epje/i2011-11129-1.

[22] Lorenz, B., et al. "Rubber Friction on Road Surfaces: Experiment and Theory for Low Sliding Speeds." *The Journal of Chemical Physics*, vol. 142, no. 19, 21 May 2015, p. 194701., doi:10.1063/1.4919221.

[23] Martin, Pamela J., et al. "SILICA-REINFORCED EPOXIDIZED NATURAL RUBBER TIRE TREADS — PERFORMANCE AND DURABILITY." *Rubber Chemistry and Technology*, vol. 88, no. 3, 2015, pp. 390–411., doi:10.5254/rct.15.85940.

[24] Maugis, D, and M Barquins. "Fracture Mechanics and the Adherence of Viscoelastic Bodies." *Journal of Physics D: Applied Physics*, vol. 11, no. 14, 1978, pp. 1989–2023., doi:10.1088/0022-3727/11/14/011.

[25] Nayak, P. Ranganath. "Random Process Model of Rough Surfaces." *Journal of Lubrication Technology*, vol. 93, no. 3, 1971, pp. 398–407., doi:10.1115/1.3451608.

[26] Pastewka, Lars, and Mark O. Robbins. "Contact between Rough Surfaces and a Criterion for Macroscopic Adhesion." *Proceedings of the National Academy of Sciences*, vol. 111, no. 9, 2014, pp. 3298–3303., doi:10.1073/pnas.1320846111.

[27] Persson, B. N. "Theory of Rubber Friction and Contact Mechanics." *The Journal of Chemical Physics*, vol. 115, no. 8, 2001, pp. 3840–3861., doi:10.1063/1.1388626.

[28] Persson, B. N. "Adhesion between Elastic Bodies with Randomly Rough Surfaces." *Physical Review Letters*, vol. 89, no. 24, 21 Apr. 2002, doi:10.1103/physrevlett.89.245502.

[29] Persson, B.N.J., et al. "On the Nature of the Static Friction, Kinetic Friction and Creep." *Wear*, vol. 254, no. 9, 2003, pp. 835–851., doi:10.1016/s0043-1648(03)00234-5.

[30] Persson, B N, et al. "On the Nature of Surface Roughness with Application to Contact Mechanics, Sealing, Rubber Friction and Adhesion." *Journal of Physics: Condensed Matter*, vol. 17, no. 1, 2004, doi:10.1088/0953-8984/17/1/r01.

[31] Persson, B N. "Rubber Friction and Tire Dynamics." *Journal of Physics: Condensed Matter*, vol. 23, no. 1, 2010, p. 015003., doi:10.1088/0953-8984/23/1/015003.

[32]   Persson, B. N. "On the Fractal Dimension of Rough Surfaces." *Tribology Letters*, vol. 54, no. 1, 2014, pp. 99–106., doi:10.1007/s11249-014-0313-4.

[33]   Persson, J. S., et al. "On the Use of Silicon Rubber Replica for Surface Topography Studies." *Tribology Letters*, vol. 66, no. 4, 2018, doi:10.1007/s11249-018-1092-0.

[34]   Popov, Valentin L. "Rubber Friction and Contact Mechanics of Rubber." *Contact Mechanics and Friction*, 2010, pp. 255–270., doi:10.1007/978-3-642-10803-7_16.

[35]   Robertson, Christopher G, et al. "A Non-Equilibrium Model for Particle Networking in Filled Elastomers." Spring 2019 Technical Meeting of the Rubber Division, ACS. Spring 2019 Technical Meeting of the Rubber Division, ACS, 2019.

[36]   Scaraggi, M, and B N Persson. "Friction and Universal Contact Area Law for Randomly Rough Viscoelastic Contacts." *Journal of Physics: Condensed Matter*, vol. 27, no. 10, 2015, p. 105102., doi:10.1088/0953-8984/27/10/105102.

[37]   Tanaka, Hiro, et al. "Prediction of the Friction Coefficient of Filled Rubber Sliding on Dry and Wet Surfaces with Self-Affine Large Roughness." *Mechanical Engineering Journal*, vol. 3, no. 1, 21 Jan. 2016, doi:10.1299/mej.15-00084.

[38]   Tiwari, A., et al. "The Effect of Surface Roughness and Viscoelasticity on Rubber Adhesion." *Soft Matter*, vol. 13, no. 19, 2017, pp. 3602–3621., doi:10.1039/c7sm00177k.

[39]   Tolpekina, T. V., and B N. J. Persson. "Adhesion and Friction for Three Tire Tread Compounds." *An Open Access Journal from MDPI*, Apollo Tyres Global R&D, 26 Feb. 2019, www.mdpi.com/journal/lubricants.

[40]   Williams, Malcolm L., et al. "The Temperature Dependence of Relaxation Mechanisms in Amorphous Polymers and Other Glass-Forming Liquids." *Journal of the American Chemical Society*, vol. 77, no. 14, 1955, pp. 3701–3707., doi:10.1021/ja01619a008.

[41]   Wurst, Brad, and Olsen, Maggie. "Tire Components 101: Building Blocks of a Radial Tire." Smithers Webinar, 2019.

[42]   Yang, C., and B. N. Persson. "Molecular Dynamics Study of Contact Mechanics: Contact Area and Interfacial Separation from Small to Full Contact." *Physical Review Letters*, vol. 100, no. 2, 2008, doi:10.1103/physrevlett.100.024303.

[43]   Zhao, J., et al. "Applicability of the Time–Temperature Superposition Principle in Modeling Dynamic Response of a Polyurea." *Mechanics of Time-Dependent Materials*, vol. 11, no. 3-4, 2007, pp. 289–308., doi:10.1007/s11043-008-9048-7.

APPENDICES

APPENDIX A

COPYRIGHT PERMISSIONS

MDPI Open Access Information and Policy

All articles published by MDPI are made immediately available worldwide under an open access license. This means:

- everyone has free and unlimited access to the full-text of *all* articles published in MDPI journals;

- everyone is free to re-use the published material if proper accreditation/citation of the original publication is given;

- open access publication is supported by the authors' institutes or research funding agencies by payment of a comparatively low Article Processing Charge (APC) for accepted articles.

Permissions

No special permission is required to reuse all or part of article published by MDPI, including figures and tables. For articles published under an open access Creative Common CC BY license, any part of the article may be reused without permission provided that the original article is clearly cited. Reuse of an article does not imply endorsement by the authors or MDPI.

Beth Darchi   Wed, Jul 21, 10:40 AM (4 days ago)
to me ▾

Dear Mr. Kelly,

This permission has been revised. It is our pleasure to grant you permission to use the ASME **Figure 4 only** from "A Simplified Version of Persson's Multiscale Theory for Rubber Friction Due to Viscoelastic Losses," by M. Ciavarella, J. Tribol. January 2018, 140(1), cited in your letter for inclusion in a thesis entitled Simplified model for rubber friction to study the effect of direct and indirect DMA test results to be published by University of Akron.

Permission is granted for the specific use as stated herein and does not permit further use of the materials without proper authorization. As is customary, we request that you ensure full acknowledgment of this material, the author(s), source and ASME as original publisher.

Many thanks for your interest in ASME publications.

Sincerely,

Beth Darchi
Publishing Administrator
ASME
2 Park Avenue, 6th Floor
New York, NY 10016-5990
darchib@asme.org

APPENDIX B

NOMENCLATURE

$C(q)$ Power spectrum of surface roughness

$S(q)$ Correction factor

$P(q)$ Relative area of real contact

q_f wavenumber to maintain full contact

Im E   Loss Modulus (MPa)

E   Complex Modulus (MPa)

H   Hurst exponent

h'_{rms} Real mean squared slope of the surface profile

erf   Error function

Greek letters

ζ Spatial magnification

μ_{visc} Hysteresis friction coefficient

μ_{const} Hysteresis friction coefficient

μ Total friction coefficient

σ_o Nominal contact stress (MPa)

τ_f Frictional shear stress (MPa)

τ_{f0} Nominal frictional shear stress (MPa)

v Poisson's ratio

v   velocity (m/s)

q   wave number

Abbreviations

DMA   Dynamic Mechanical Analysis

HFDMA   High frequency dynamic mechanical analysis

TTS   Time-temperature superposition

WLF   Williams, Landel, and Ferry